

Supplementary Information

Highly Efficient Color-Tunable Organic Co-crystals Unveiling Polymorphism, Isomerism, Delayed Fluorescence for Optical Waveguides and Cell-imaging

Debasish Barman¹, Mari Annadhasan², Anil Parsram Bidkar³, Pachaiyappan Rajamalli⁴, Debika Barman,¹ Siddhartha Sankar Ghosh^{5,6*}, Rajadurai Chandrasekar^{2*} & Parameswar Krishnan Iyer^{1,6*}

¹Department of Chemistry, Indian Institute of Technology Guwahati, Guwahati-781039, India.

²School of Chemistry, and Centre for Nanotechnology University of Hyderabad, Gachibowli, Prof. C. R. Rao Road, Hyderabad-500046, India.

³Department of Radiology and Biomedical Imaging, University of California, San Francisco, San Francisco, California 94143, United States.

⁴Materials Research Centre, Indian Institute of Science Bangalore-560012, India.

⁵Department of Bioscience and Bioengineering IIT Guwahati, Guwahati, Assam, India.

⁶Centre for Nanotechnology, Indian Institute of Technology Guwahati, Guwahati-781039, India.

*e-mail: pki@iitg.ac.in

*e-mail: r.chandrasekar@uohyd.ac.in

*e-mail: sghosh@iitg.ac.in

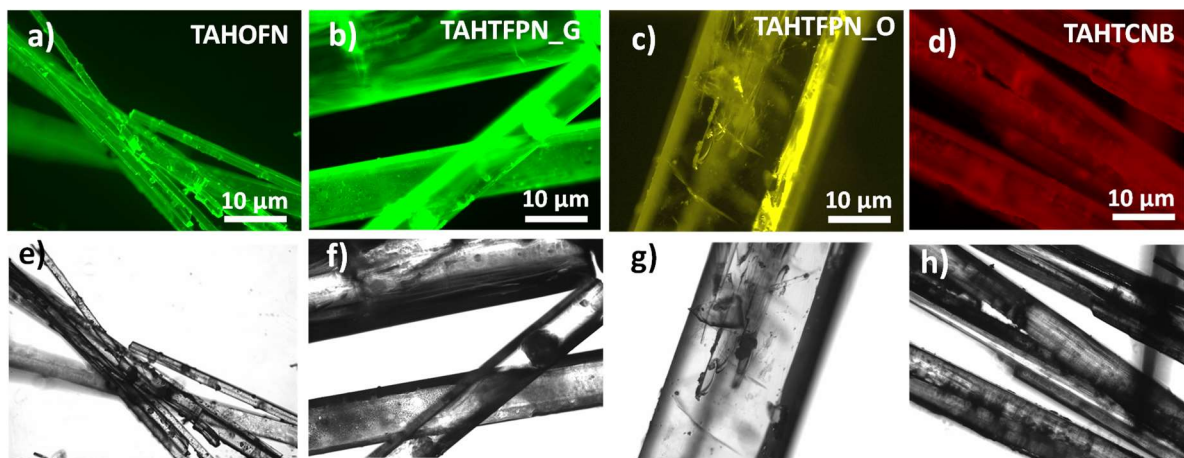
Supplementary Table of Contents

Title	Page No
Supplementary Fig. 1. Fluorescence Microscope images of the prepared co-crystals.	S5
Supplementary Fig. 2. FTIR spectra of TAH crystals (green line), OFN (orange line) and TAHOFN (red line).	S5
Supplementary Fig. 3. FTIR spectra of TAH crystals (green line), TFPN (yellow line) and TAHTFPN_G (black line).	S6
Supplementary Fig. 4. FTIR spectra of TAH crystals (green line), TFPN (yellow line) and TAHTFPN_O (black line).	S6

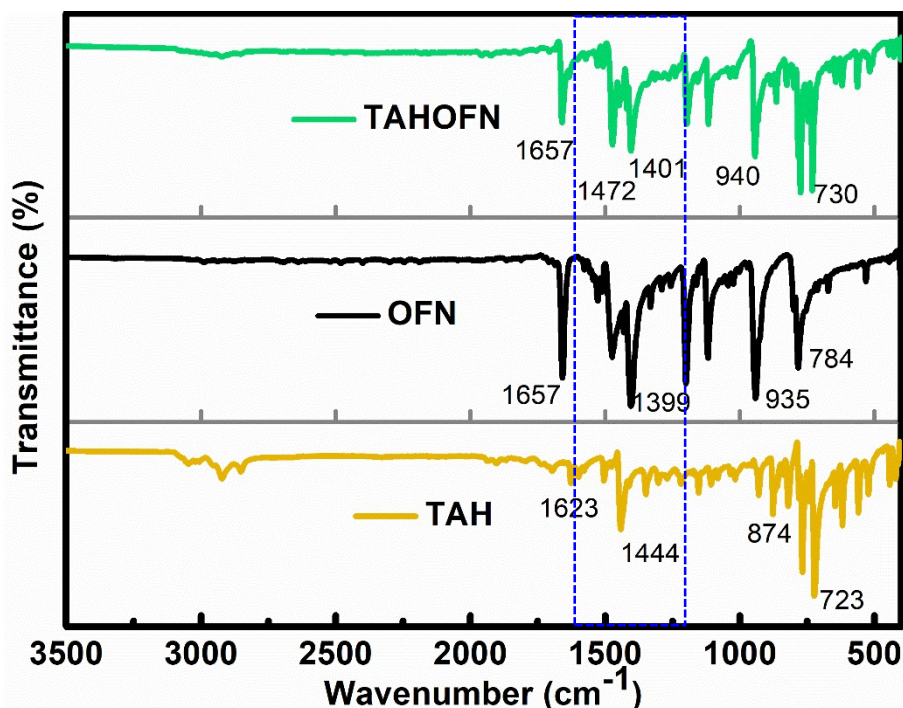
Supplementary Fig. 5. FTIR spectra of TAH crystals (green line), TCNB (yellow line) and TAHTCNB (black line).	S7
Supplementary Fig. 6. Raman spectra of TAH (deep green line) OFN (orange line) and TAHOFN (red line).	S7
Supplementary Fig. 7. Raman spectra of TAH (deep green line) TFPN (greenish yellow line) and TAHTFPN_G (black line).	S8
Supplementary Fig. 8. Raman spectra of TAH (deep green line) TFPN (greenish yellow line) and TAHTFPN_O (black line).	S8
Supplementary Fig. 9. Raman spectra of TAH (deep green line) TCNB (greenish yellow line) and TAHTCNB (black line).	S9
Supplementary Fig. 10. Experimental PXRD pattern for TAH (green line), OFN (orange line) and TAHOFN with calculated PXRD (red lines).	S9
Supplementary Fig. 11. Experimental PXRD pattern for TAH (green line), TFPN (yellow line) and TAHTFPN_G with calculated PXRD (black lines).	S10
Supplementary Fig. 12. Experimental PXRD pattern for TAH (green line), TFPN (yellow line) and TAHTFPN_O with calculated PXRD (black lines).	S10
Supplementary Fig. 13. Experimental PXRD pattern for TAH (green line), TCNB (yellow line) and TAHTCNB with calculated PXRD (black lines).	S11
Supplementary Fig. 14. Thermal gravimetric analysis (TGA) study for TAH (green line), OFN (yellow line) and TAHOFN (black lines).	S11
Supplementary Fig. 15. Thermal gravimetric analysis (TGA) study for TAH (green line), TFPN (yellow line) and TAHTFPN (black lines).	S12
Supplementary Fig. 16. Thermal gravimetric analysis (TGA) study for TAH (green line), TFPN (yellow line) and TAHTFPN_O (black lines).	S12
Supplementary Fig. 17. Thermal gravimetric analysis (TGA) study for TAH (green line), TCNB (yellow line) and TAHTCNB (black lines).	S13
Supplementary Fig. 18. Differential scanning calorimetry (DSC) study for TAHOFN, TAHTFPN_G, TAHTFPN_O and TAHTCNB respectively.	S13
Supplementary Fig. 19. Stacked ¹ H NMR spectra for TAHOFN, TAHTFPN and TAHTCNB co-crystals, recorded in DMSO-d ₆ and D ₂ O mixture at 298K.	S14
Supplementary Table 1-4. Calculated attachment energies of different crystal facets of TAHOFN, TAHTFPN_G, TAHTFPN_O, TAHTCNB co-assembly.	S14-S15
Supplementary Table 5. Crystallographic data and structure refinement parameters of TAHOFN, TAHTFPN_G, TAHTFPN_O and TAHTCNB co-crystals.	S16
Supplementary Fig. 20. Twisted angle between two planes of planar TAH and central phenyl planes in difference interactive orientation to the guest molecules (OFN, TFPN and TCNB)	S17
Supplementary Fig. 21. Unit-cell packing in the SC-XRD structure for TAHOFN, TAHTFPN_G, TAHTFPN_O, TAHTCNB showing close contact with mixed stack and segregated stack alignment between TAH and OFN, TFPN and TCNB cores.	S17
Supplementary Fig. 22. Supramolecular bulk assembly of TAHOFN, TAHTFPN_G, TAHTFPN_O and cis-TAHTCNB	S18

Supplementary Table 6. SCXRD-crystal structural analysis with non-covalent interactions and dihedral angle for all the afforded co-crystals.	S18
Supplementary Fig. 23-26. 2D Finger print for surface to atom intermolecular interactions mapped on Hirshfeld surface in TAHOFN, TAHTFPN_G, TAHTFPN_O and TAHTCNB.	S19-S20
Supplementary Fig. 27. Orientation of dipole moment (μ) and pitch angles between D-A obtained from TD-DFT and SC-XRD structures of TAHOFN, TAHTFPN_G, TAHTFPN_O and TAHTCNB.	S21
Supplementary Fig. 28. Solid state UV-visible spectra of TAHOFN, TAHTFPN_G, TAHTFPN_O and TAHTCNB co-crystals.	S21
Supplementary Fig. 29. Photophysical and morphological characterization of TAH donor.	S22
Supplementary Fig. 30. FETEM images (inset: DLS graph for size distribution) of co-crystal nano aggregates formed in DMSO/H ₂ O (99%, f_w) for TAHOFN, TAHTFPN_G and TAHTCNB	S22
Supplementary Fig. 31-33. Zeta-potential recorded in H ₂ O for TAHOFN, TAHTFPN_G and TAHTCNB at 10^{-5} M concentration.	S23-S24
Supplementary Fig. 34-37. PLQY measurement for TAHOFN, TAHTFPN_G, TAHTFPN_O and TAHTCNB co-crystals.	S24-S26
Supplementary Table 7-10. Time resolved PL Decay of TAHOFN, TAHTFPN_G, TAHTFPN_O and TAHTCNB co-crystal $\lambda_{\text{Ex.}}$ 405 nm and $\lambda_{\text{Em.}}$ 540, 545, 560 and 590 nm.	S26-S27
Supplementary Fig. 38. a) Temperature dependent delayed emission spectra for TAHTCNB co-crystal in solid state. b) PL at RT and phosphorescence at 77K. c) Steady state PL at RT and 77K for TAHTCNB solid state (powder).	S28
Supplementary Table 11-13. Fitting results for delayed decay at 300, 200 and 100K for TAHTCNB co-crystal.	S28-S29
Supplementary Fig. 39-42. Cyclic voltammetry curves of TAH crystals (green line), OFN, TFPN, TCNB (orange/yellow line) and TAHOFN, TAHTFPN_G, TAHTCNB_O and TAHTCNB (red/black line).	S29-S31
Supplementary Table 14. The energy levels calculated from cyclic voltammetry and DFT.	S32
Supplementary Fig. 43-46. Natural transition orbitals (NTOs) for lowest excited singlet and triplet excited states for TAHOFN, TAHTFPN_G, TAHTFPN_O and TAHTCNB.	S32-S34
Supplementary Fig. 37. Mechanism of weak fluorescence (a-PET & d-PET) for TAHOFN by DFT/TD-DFT calculated HOMO/LUMO energy band diagram for conformer TAH and OFN.	S34

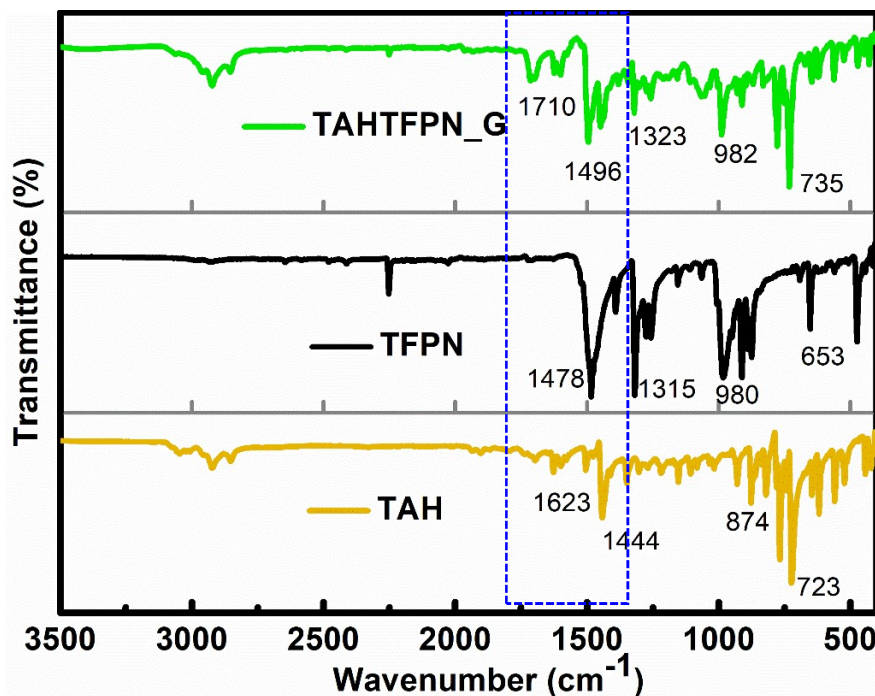
Supplementary Fig. 48. Color-tunable fluorescence and CT mechanism for the polymorphic co-crystals of TAHTFPN_G and TAHTFPN_O by DFT/TD-DFT calculated HOMO/LUMO energy band diagram for the conformer TAH and TFPN.	S35
Supplementary Fig. 49. Red fluorescence and strong narrow band CT mechanism for the cis-isomeric co-crystals of TAHTCNB by DFT/TD-DFT calculated HOMO/LUMO energy band diagram for the conformer TAH and TCNB.	S35
Supplementary Table 15-22. Vertical energy transitions with major frontier orbital contribution for TAHOFN, TAHTFPN_G, TAHTFPN_O and TAHTCNB cocrystals at B3LYP/6-31G(d,p) level for singlet and triplet states.	S36-S40
Supplementary Table 23. SOC-matrix element (SOCME) calculated by using ORCA 4.5.0 software with ORCA_SOC module	S41
Supplementary Fig. 50. Electron spin resonance (ESR) spectra for TAH (yellow line), TAHOFN (off green line), TAHTFPN_G (green line) and TAHTCNB (red line).	S41
Supplementary Fig. 51. Chemical structures of OFN, TFPN and TCNB molecule, where x, y, and z are the bond length of carbon-carbon bond at neutral state.	S42
Supplementary Fig. 52-54. Spatially resolved spectra of TAHOFN, TAHTFPN and TAHTCNB crystal: Excitation position was kept constant and PL signals were collected at different positions.	S42-S43
Supplementary Fig. 55-57. Z-stacking analysis of the MCF-7, confirming the internalization and localization of the TAHOFN in the cytoplasm. (Scale bar: 5 μm).	S44-S45
Supplementary Fig. 58. Cellular internalization mechanism studies using co-crystals.	S45
Supplementary Table 24. A brief summary of the previous report on various optically waveguide active molecular crystals	S46-S49
Supplementary Fig. 59-62. An ellipsoid figure of TAHTCNB single crystal structure.	S50-S51
Supplementary Table 25-28. Cartesian coordinates of TAHOFN, TAHTFPN_G, TAHTFPN_O and TAHTCNB used for the TD-DFT calculation at B3LYP/6-31G (d,p) level.	S52-S60
Supplementary Reference	S61



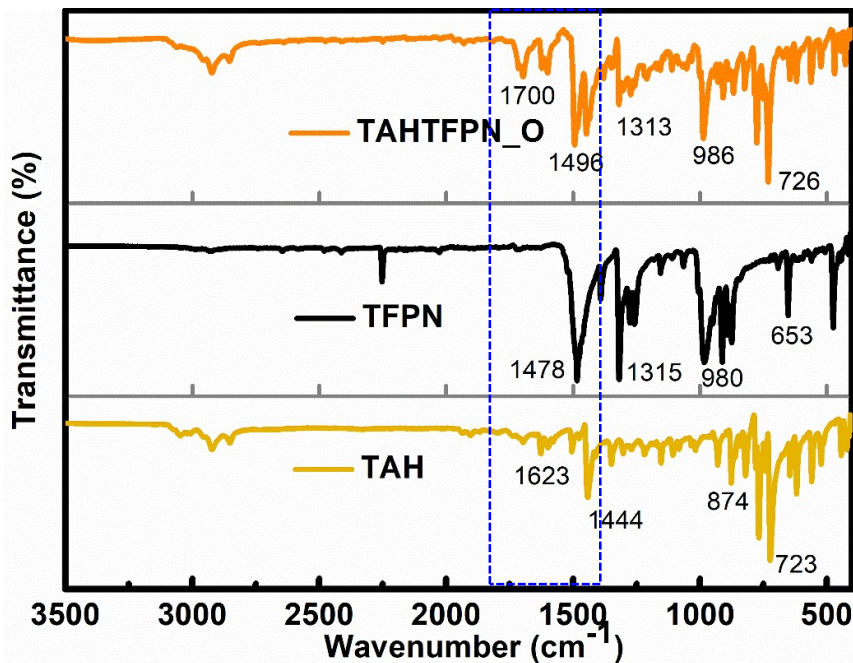
Supplementary Fig. 1: (a-d) Fluorescence microscopy images for TAHOFN, TAHTFPN_G, TAHTFPN_O and TAHTCNB co-crystals with the excitation wavelength 405 nm. (e-h) While at the bottom images are their corresponding bright field images (scale bar: 10 μm).



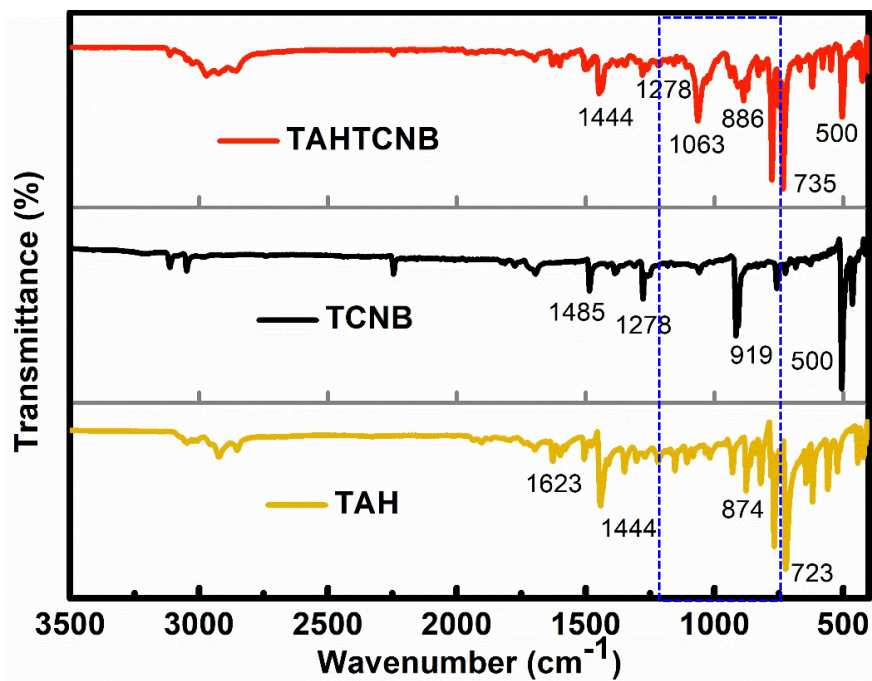
Supplementary Fig. 2: FTIR spectra of TAH crystals (yellow line), OFN (black line) and TAHOFN (green line). Here, the C-F stretching vibration peak in OFN at 1399 cm^{-1} became strong and shifted to 1401 cm^{-1} , while C-H bending frequency of TAH peaks at 1444 cm^{-1} shifted to 1472 cm^{-1} .



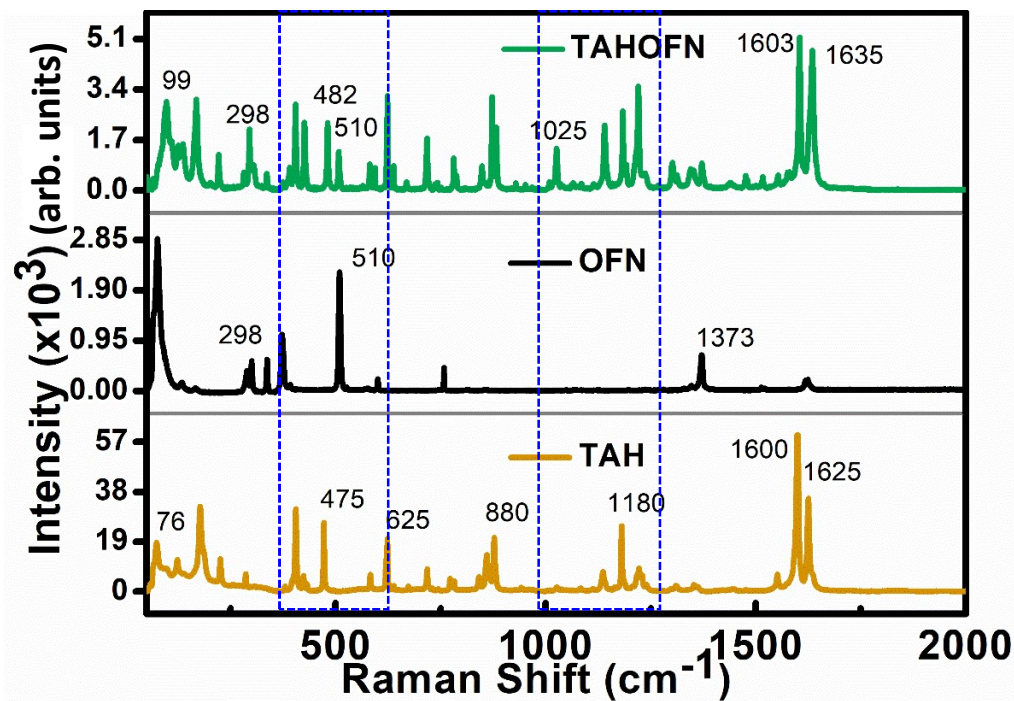
Supplementary Fig. 3: FTIR spectra of TAH crystals (yellow line), TFPN (black line) and TAHTFPN_G (green line). Co-crystal TAHTFPN_G, the peak of C-F stretching vibration in TFPN at 1315 cm^{-1} became strong and shifted to 1323 cm^{-1} , while C-H bending frequency of TAH in co-crystal, peaks at 1472 cm^{-1} shifted to 1496 cm^{-1} .



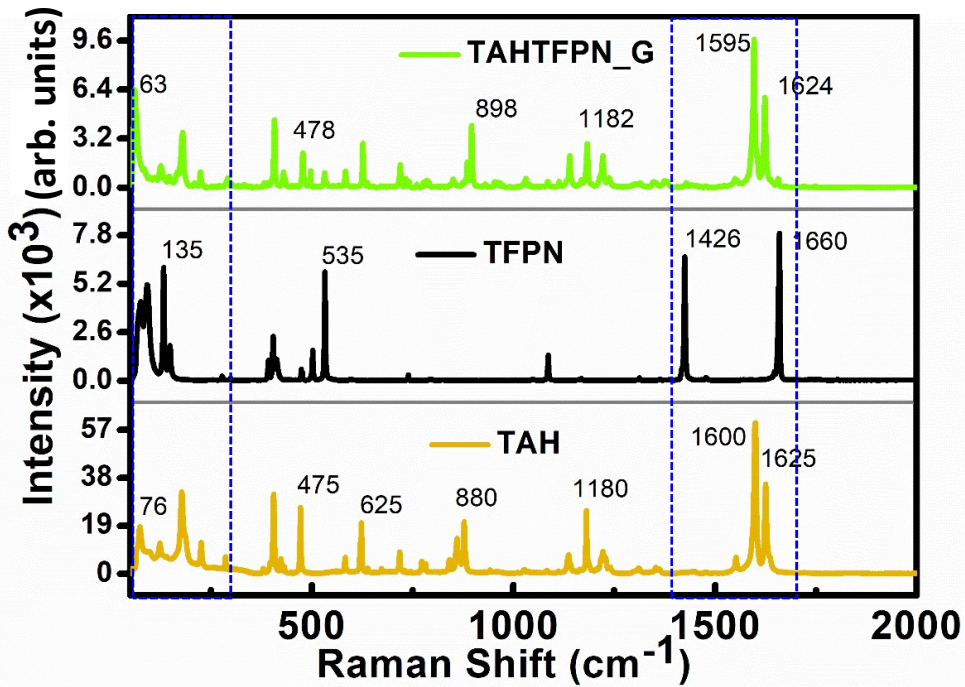
Supplementary Fig. 4: FTIR spectra of TAH crystals (yellow line), TFPN (black line) and TAHTFPN_O (orange line). Co-crystal TAHTFPN_O, the peak of C-F stretching vibration in TFPN at 1315 cm^{-1} became strong and shifted to 1313 cm^{-1} while C-H bending frequency of TAH in co-crystal, peaks at 1472 cm^{-1} shifted to 1496 cm^{-1} .



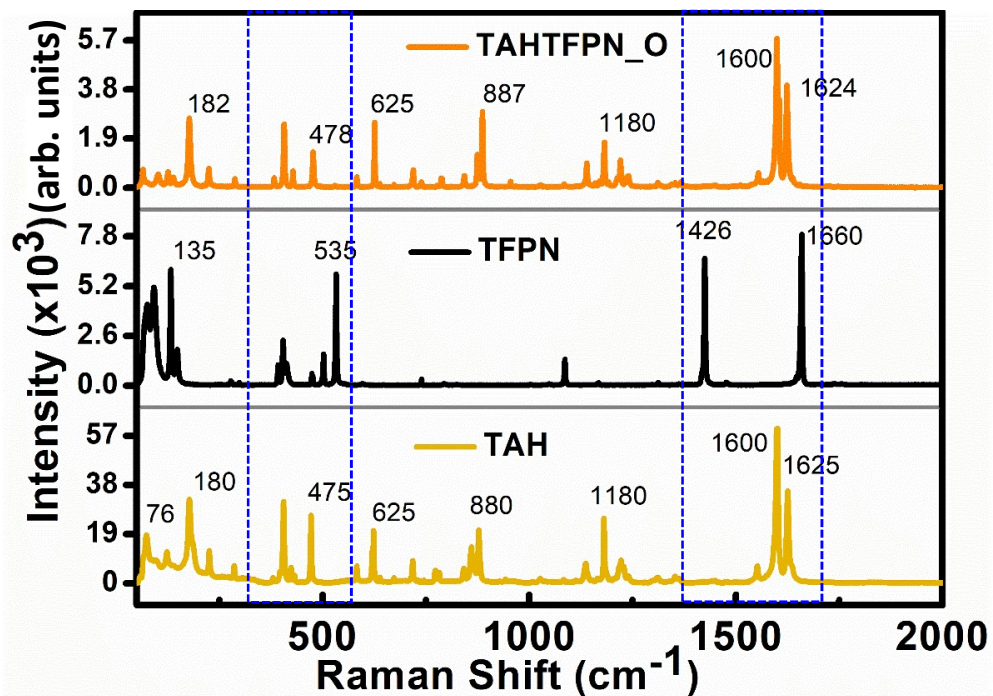
Supplementary Fig. 5: FTIR spectra of TAH crystals (yellow line), TCNB (black line) and TAHTCNB (red line).. Co-crystal TAHTCNB no significant CN stretching vibration shift occurred; however, C-H stretching frequency at 919 cm^{-1} shifted to 886 cm^{-1} and became weak. Further, a new peak also appeared at 1063 cm^{-1} , which could be due to the strong CT-complexation.



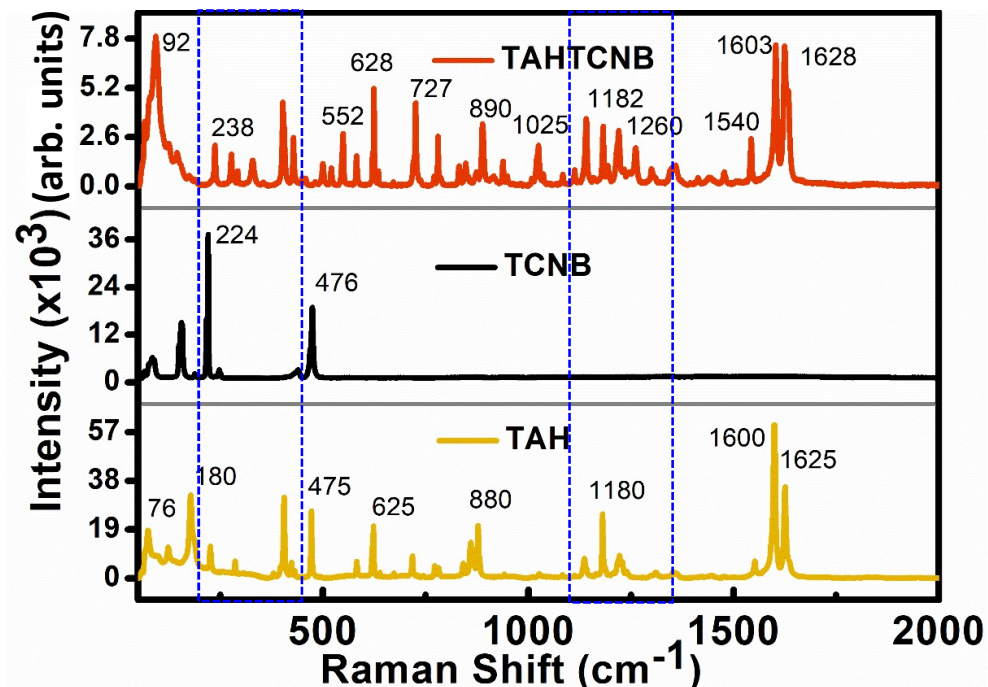
Supplementary Fig. 6: Raman spectra of TAH crystals (yellow line), OFN (black line) and TAHOFN (green line).



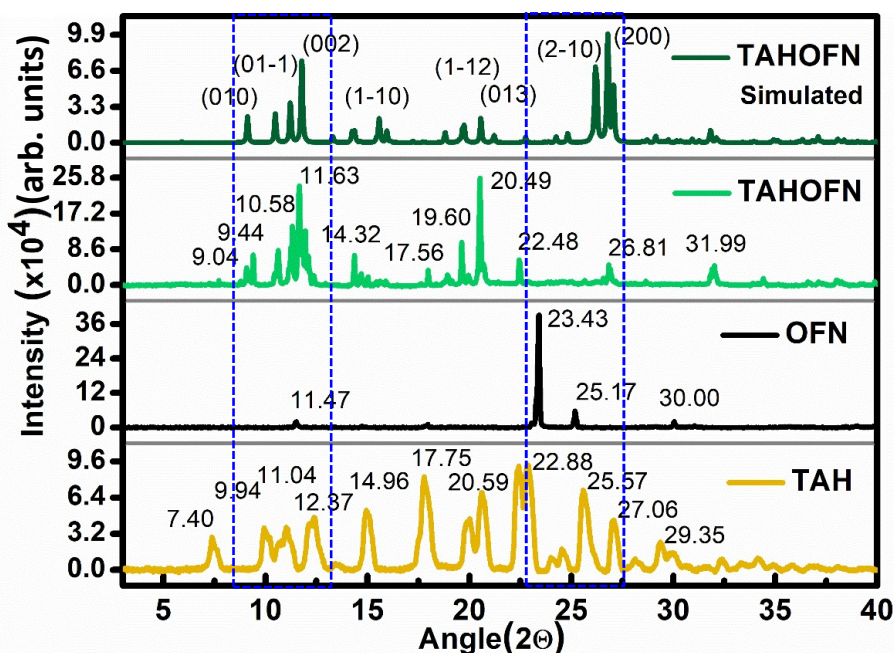
Supplementary Fig. 7: Raman spectra of TAH crystals (yellow line), TFPN (black line) and TAHTFPN_G (green line).



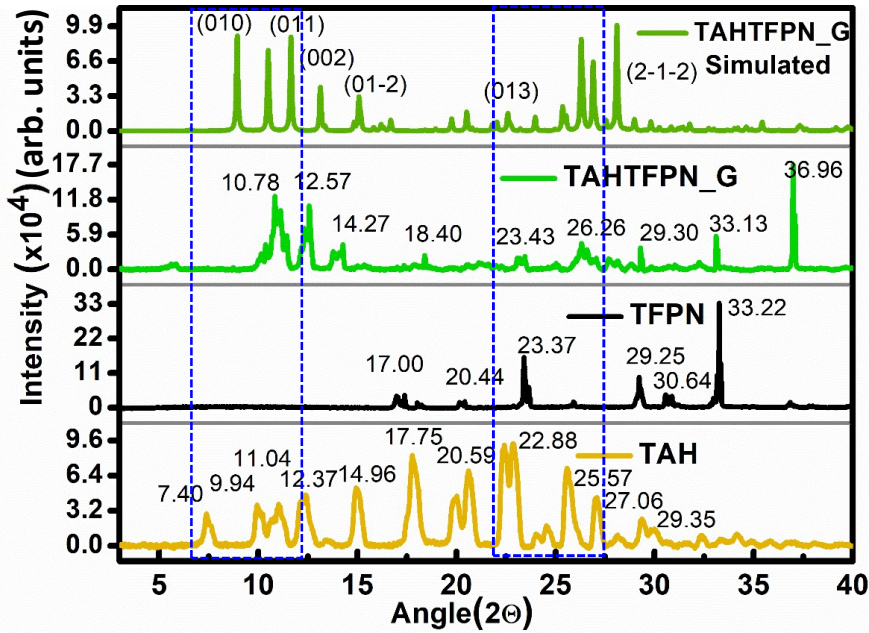
Supplementary Fig. 8: Raman spectra of TAH crystals (yellow line), TFPN (black line) and TAHTFPN_O (orange line).



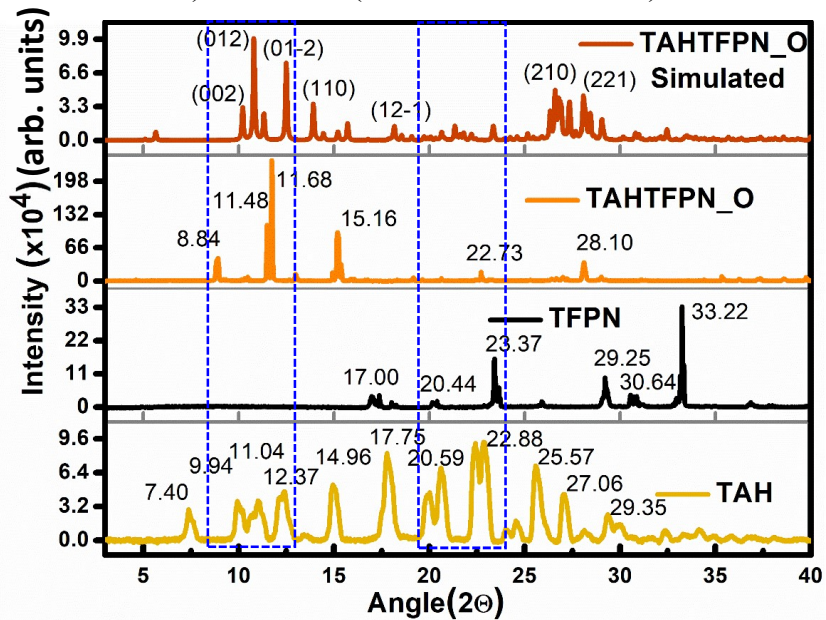
Supplementary Fig. 9: Raman spectra of TAH crystals (yellow line), TCNB (black line) and TAHTCNB (red line).



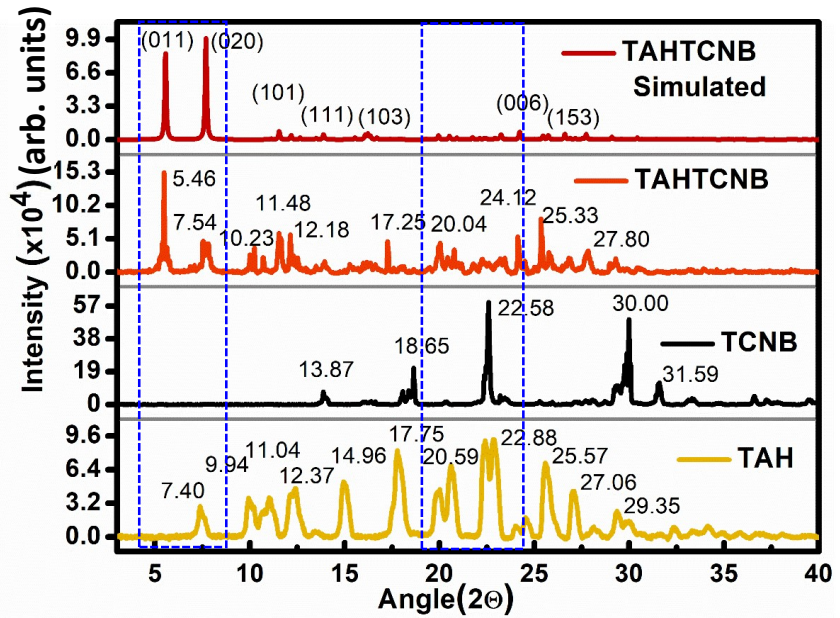
Supplementary Fig. 10: Experimental PXRD pattern for TAH crystals (yellow line), OFN (black line), experimental TAHOFN (green line) and simulated TAHOFN (dark green line). Appearance of several new characteristic peaks in TAHOFN co-crystals (9.44°, 11.63°, 14.32°, 19.60°, 22.48°, 31.99°), whereas the absence of several original peaks from pure TAH (7.40°, 12.37°, 17.75°, 22.88°, 27.06°), OFN (23.43°, 25.17°, 30.00°).



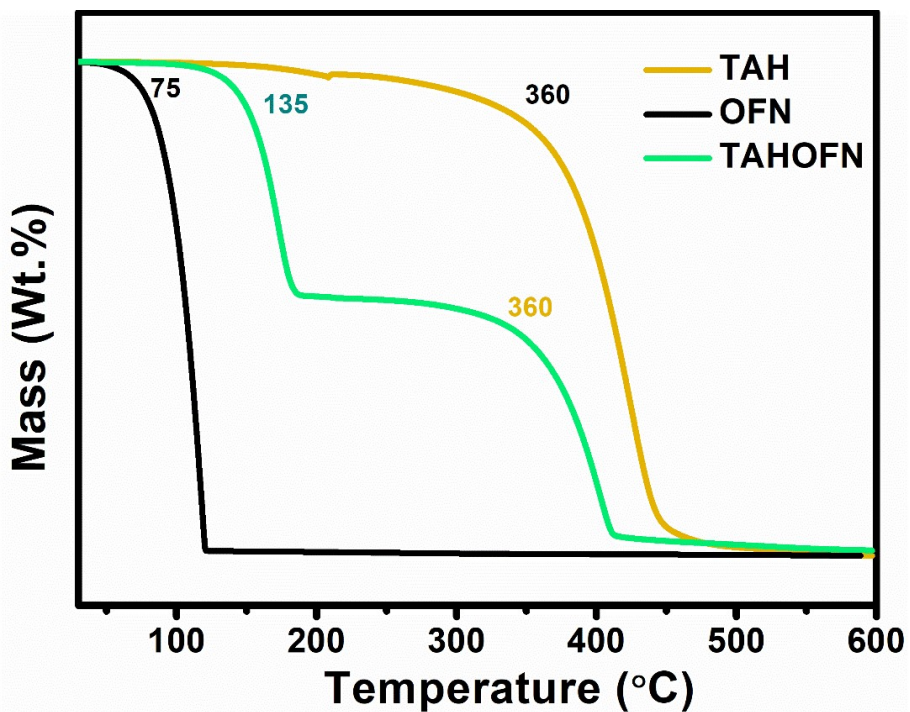
Supplementary Fig. 11: Experimental PXRD pattern for TAH crystals (yellow line), TFPN (black line), experimental TAHTFPN_G (green line) and simulated TAHTFPN_G (yellow green line). Appearance of several new characteristic peaks in TAHTFPN_G co-crystals 10.78°, 12.57°, 18.40°, 26.26°, 36.96° and the absence of several original peaks from pure TAH (7.40°, 12.37°, 17.75°, 22.88°, 27.06°) and TFPN (17.00°, 23.37°, 33.22°).



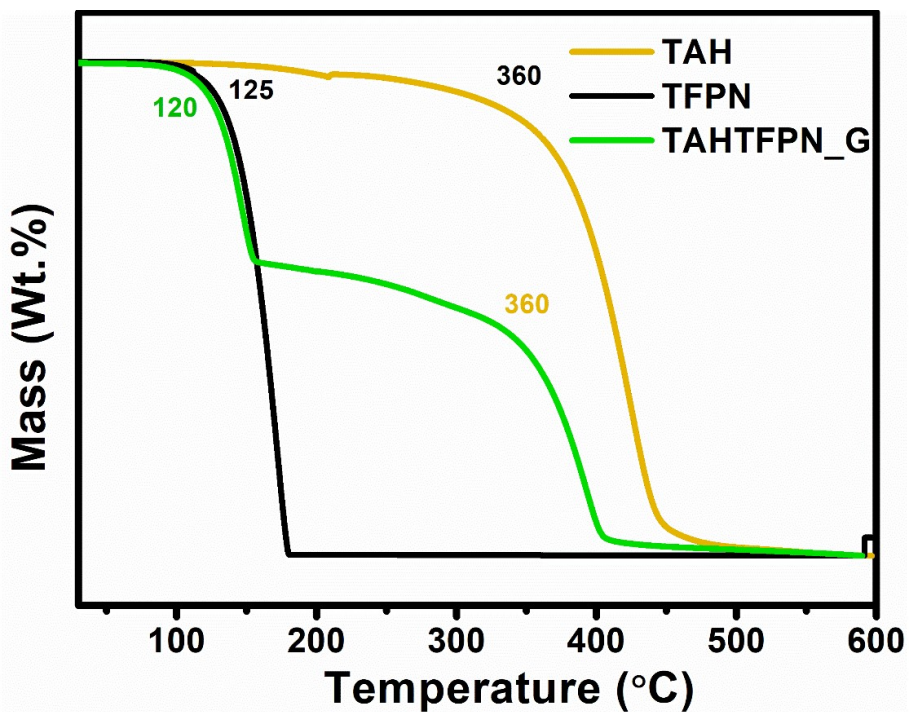
Supplementary Fig. 12: Experimental PXRD pattern for TAH crystals (yellow line), TFPN (black line), experimental TAHTFPN_O (orange line) and simulated TAHTFPN_O (dark yellow line). Appearance of several new characteristic peaks in TAHTFPN_O co-crystals at 8.84°, 11.48°, 11.68°, 15.16°, 22.73°, 28.10° and the absence of several original peaks from pure TAH (7.40°, 12.37°, 17.75°, 22.88°, 27.06°), and TFPN (17.00°, 23.37°, 33.22°).



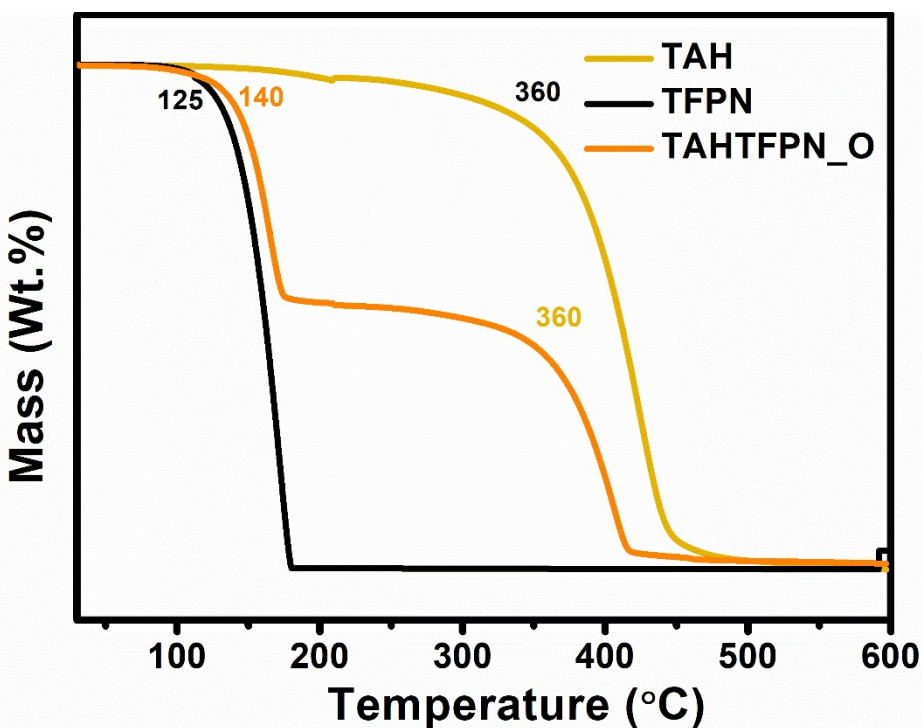
Supplementary Fig. 13: Experimental PXRD pattern for TAH crystals (yellow line), TCNB (black line), experimental TAHTCNB (red line) and simulated TAHTCNB (dark red line). Appearance of several new characteristic peaks in TAHTCNB co-crystals of 5.46°, 7.54°, 11.48°, 17.25°, 24.12°, 27.80° and the absence of several original peaks from pure TAH (7.40°, 12.37°, 17.75°, 22.88°, 27.06°), and TCNB (18.65°, 22.58°, 30.00°).



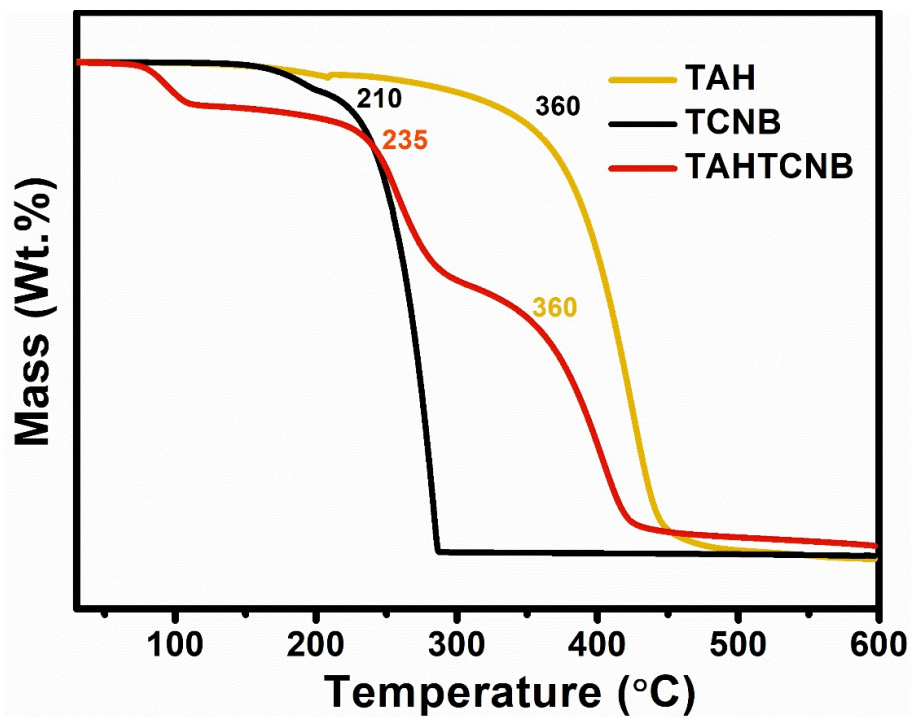
Supplementary Fig. 14: Thermal gravimetric analysis (TGA) for TAH (yellow line), OFN (black line) and TAHOFN (green line).



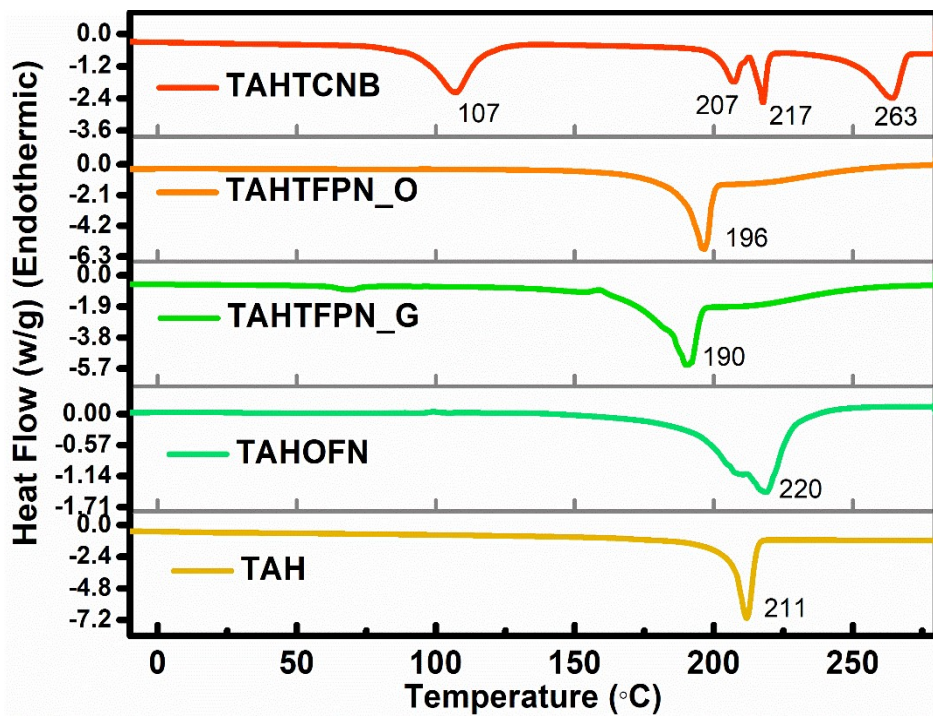
Supplementary Fig. 15: Thermal gravimetric analysis (TGA) for TAH (yellow line), TFPN (black line) and TAHTFPN_G (green line).



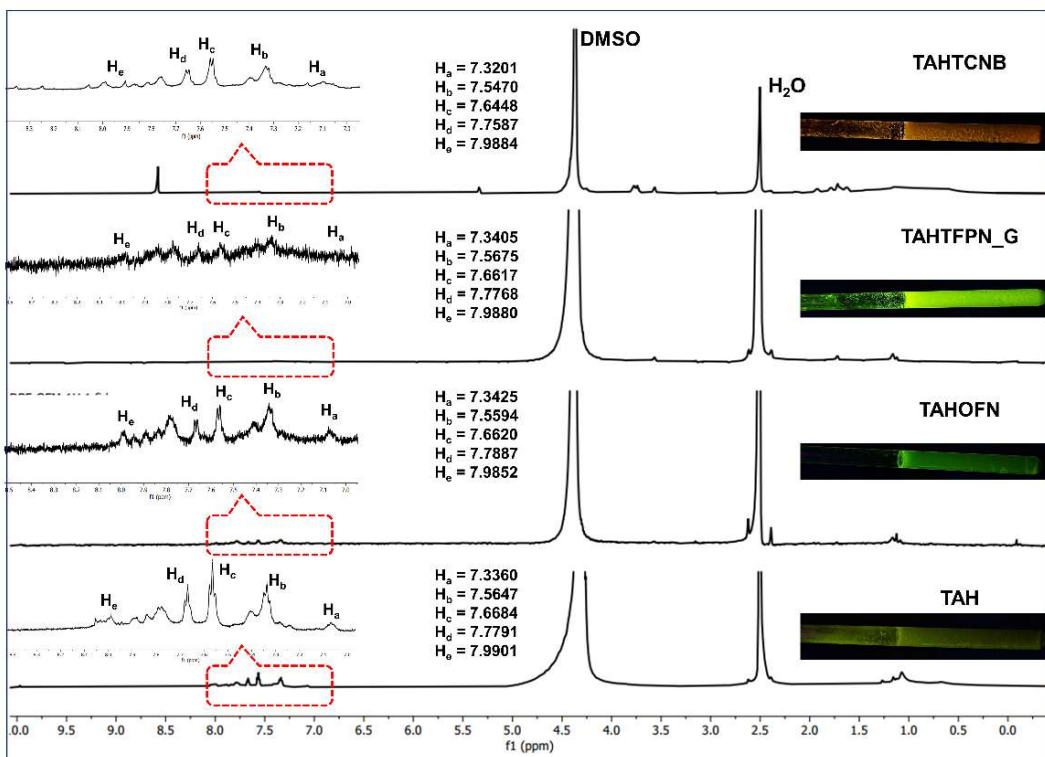
Supplementary Fig. 16: Thermal gravimetric analysis (TGA) for TAH (yellow line), TFPN (black line) and TAHTFPN_O (orange line).



Supplementary Fig. 17: Thermal gravimetric analysis (TGA) for TAH (yellow line), TCNB (black line) and TAHTCNB (red line).



Supplementary Fig. 18: Differential scanning calorimetry (DSC) study for TAH (yellow line), TAHOFN (off green line), TAHTFPN_G (green line), TAHTFPN_O (orange line) and TAHTCNB (red line).



Supplementary Fig. 19: Stacked ^1H NMR spectra for TAHOFN, TAHTFPN and TAHTCNB co-crystals, recorded in $\text{DMSO}-d_6$ and D_2O mixture at 298K. (Inset: images of NMR tubes containing co-crystals taken under 365 nm UV lamp)

Supplementary Table 1. Calculated attachment energies of different crystal facets of TAHOFN co-crystal.¹

hkl	Dhkl/Å	Eatt(Total)/kcal mol ⁻¹	Eatt(vdW)/kcal mol ⁻¹	% Total facet area
{ 0 0 1 }	15.0063956	-15.18404728	-13.11742205	54.04771092
{ 0 1 0 }	9.68802304	-36.38145248	-32.67298273	15.00237552
{ 0 1 1 }	7.8767392	-32.25494214	-29.52227144	9.5240967
{ 1 0 0 }	6.65484113	-47.72987075	-42.12068768	5.6110776
{ 1 0 -1 }	6.58258643	-45.92078761	-39.57714372	9.48065437

Supplementary Table 2. Calculated attachment energies of different crystal facets of TAHTFPN_G co-crystal.¹

hkl	Dhkl/Å	Eatt(Total)/kcal mol ⁻¹	Eatt(vdW)/kcal mol ⁻¹	% Total facet area
{ 0 0 1}	13.47278056	-18.0184494	-15.36076162	47.0257642
{ 0 1 0}	9.89148587	-36.2122139	-31.10511264	17.28027921
{ 0 1 1}	7.59166391	-30.89557461	-27.07515935	12.45274387
{ 1 0 0}	6.97242549	-45.30159773	-36.49290066	11.83982621
{ 1 0 -1}	6.6237172	-44.90672448	-36.92410463	8.8037205

Supplementary Table 3. Calculated attachment energies of different crystal facets of TAHTFPN_O co-crystal.¹

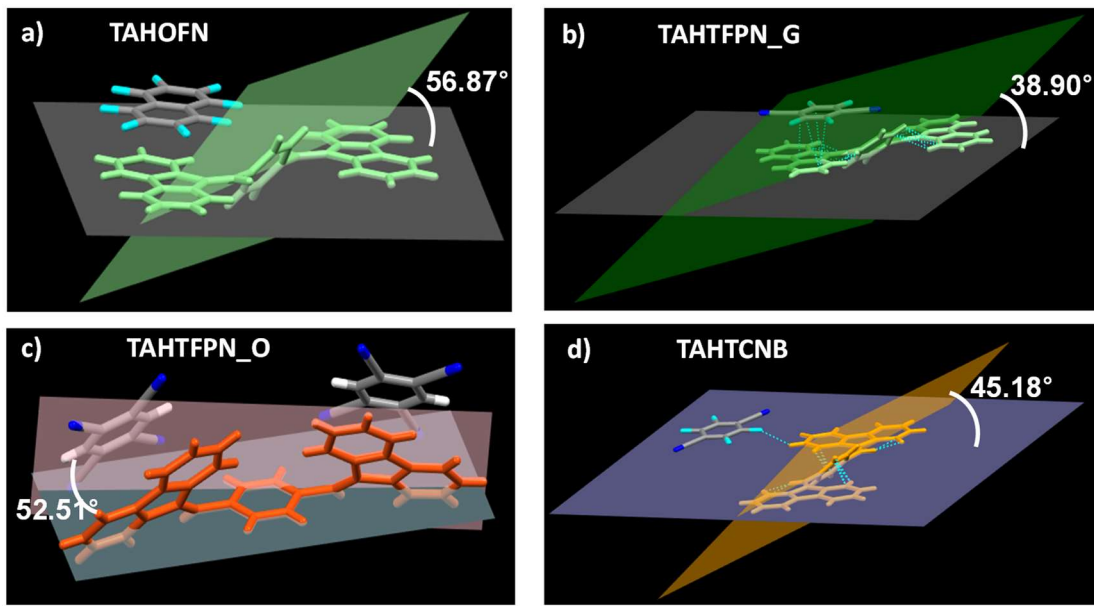
hkl	Dhkl/Å	Eatt(Total)/kcal mol ⁻¹	Eatt(vdW)/kcal mol ⁻¹	% Total facet area
{ 0 0 1}	17.30647421	-43.66871097	-32.54464608	36.04655729
{ 0 1 0 }	15.60484159	-33.75079862	-31.07773417	46.67710968
{ 1 0 0 }	6.76187634	-91.92433018	-75.2539478	16.69519411
{ 1 1 1}	6.12567428	-104.9041868	-82.94611497	0.58113891

Supplementary Table 4. Calculated attachment energies of different crystal facets of TAHTCNB co-crystal.¹

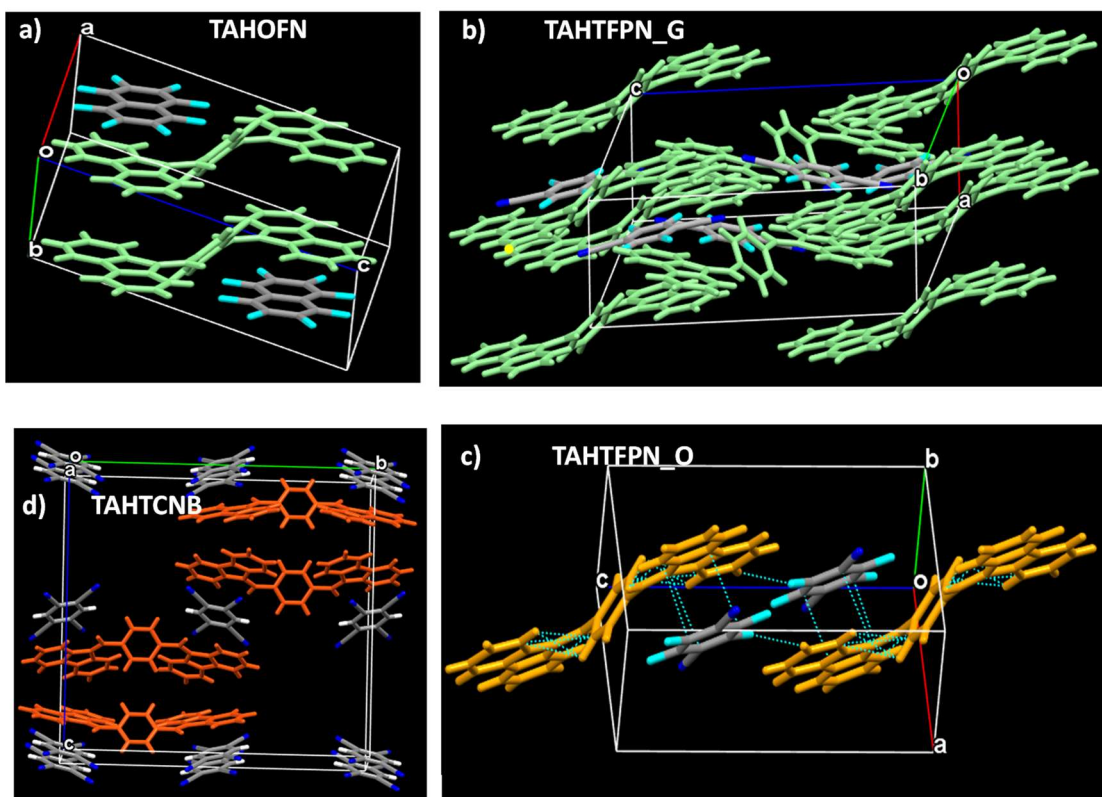
hkl	Dhkl/Å	Eatt(Total)/kcal mol ⁻¹	Eatt(vdW)/kcal mol ⁻¹	% Total facet area
{ 0 1 1}	15.89762085	-33.06173254	-26.3911915	85.99938491
{ 1 0 1}	7.65609364	-109.5026191	-69.24039722	14.00061509

Supplementary Table 5. Crystallographic data and structure refinement parameters of TAHOFN, TAHTFPN_G, TAHTFPN_O and TAHTCNB co-crystals.

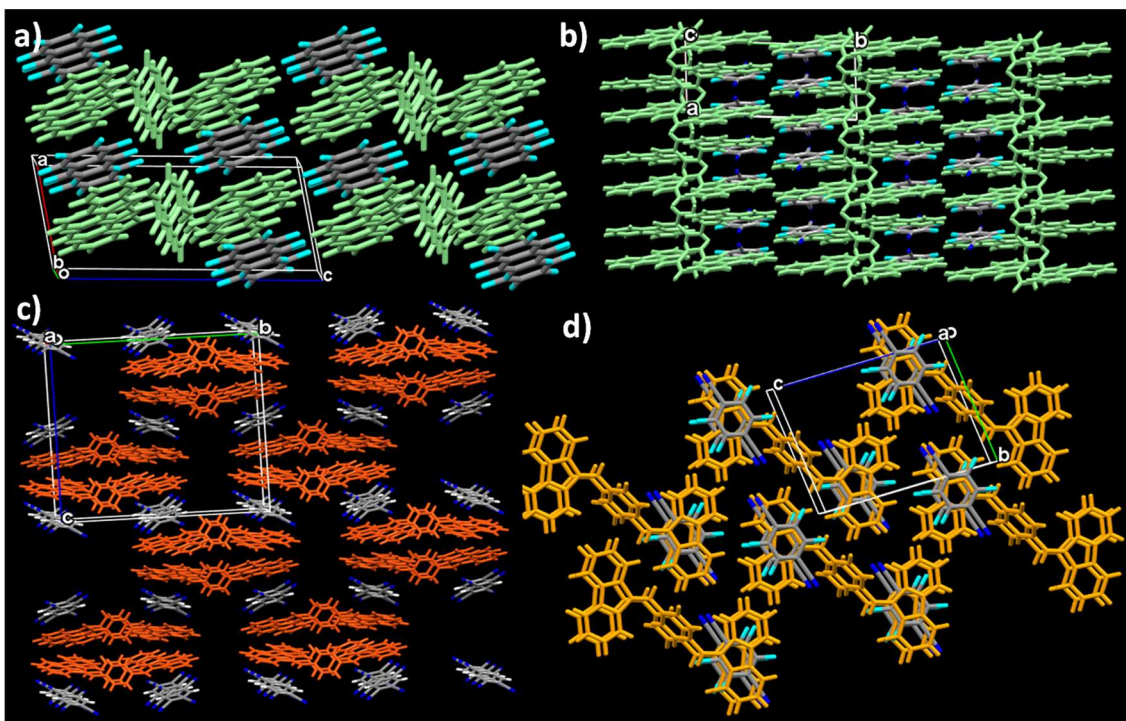
Compound	TAHOFN	TAHTFPN_G	TAHTFPN_O	TAHTCNB
Empirical formula	C ₄₄ H ₂₂ F ₈	C ₄₂ H ₂₄ F ₄ N ₂	C ₄₂ H ₂₄ F ₄ N ₂	C ₄₄ H ₂₄ N ₄
CCDC NO	2109333	2109336	2109335	2109337
Temperature/K	293 (2)	293 (2)	293 (2)	293 (2)
Crystal system	triclinic	triclinic	triclinic	orthorhombic
Space group	P -1	P -1	P -1	P n m a
a/Å	6.9672(6)	7.0777(7)	6.777(4)	8.1658(6)
b/Å	9.9719(12)	9.9789(12)	15.869(11)	22.9815(16)
c/Å	15.3125(11)	13.6987(13)	17.567(9)	22.0149(19)
α/°	91.687(8)	95.475(9)	80.15(5)	90
β/°	100.664(7)	98.390(8)	88.60(4)	90
γ/°	103.036(9)	94.383(9)	86.25(5)	90
Volume/Å ³	1015.72(17)	948.77(18)	1857.2(19)	4131.4(6)
Z	2	2	2	4
ρ _{calc} mg/mm ³	1.595	1.454	1.514	0.979
m/mm ⁻¹	0.144	0.114	1.022	0.058
F(000)	490	422	860	1264.4830
Index ranges	-8 ≤ h ≤ 7, -11 ≤ k ≤ 11, -18 ≤ l ≤ 18	-9 ≤ h ≤ 8, -11 ≤ k ≤ 13, -18 ≤ l ≤ 18	-7 ≤ h ≤ 7, -17 ≤ k ≤ 17, -19 ≤ l ≤ 19	-6 ≤ h ≤ 9, -27 ≤ k ≤ 13, -17 ≤ l ≤ 26
Reflections collected	6600	7707	44322	10016
Independent reflections	3593[R(int) = 0.0726]	4310[R(int) = 0.0799]	5355[R(int) = 0.1135]	3732
Data/restraints/parameters	3593/0/316	4310/0/280	5355/0/559	3732/0/217
Goodness-of-fit on F ²	1.060	1.081	1.238	1.0477
Final R indexes [I>=2σ (I)]	R1 = 0.0692, wR2 = 0.1610	R1 = 0.0847, wR2 = 0.2073	R1 = 0.1426, wR2 = 0.2831	R1 = 0.1207, wR2 = 0.3363
Final R indexes [all data]	R1 = 0.1424, wR2 = 0.2120	R1 = 0.1307, wR2 = 0.2466	R1 = 0.1520, wR2 = 0.2888	R1 = 0.1796, wR2 = 0.3792



Supplementary Fig. 20: Twisted angle between two planes of planar TAH and central phenyl planes in difference interactive orientation to the guest molecules (OFN, TFPN and TCNB) resulted in variable conformations of TAH, revealing polymorphism features of all the afforded co-crystals of (a) TAHOFN, (b) TAHTFPN_G, (c) TAHTFPN_O, (d) TAHTCNB.



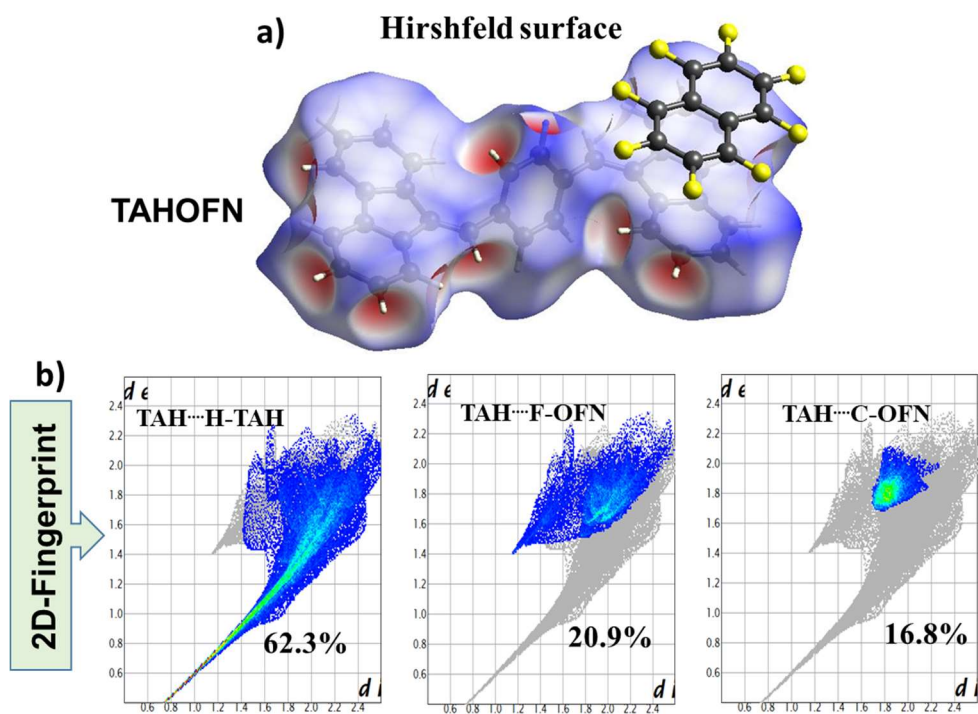
Supplementary Fig. 21: Unit cell packing in the SC-XRD structure for (a) TAHOFN, (b) TAHTFPN_G, (c) TAHTFPN_O, (d) TAHTCNB showing close contact with mixed stack and segregated stack alignment between TAH and OFN, TFPN and TCNB cores.



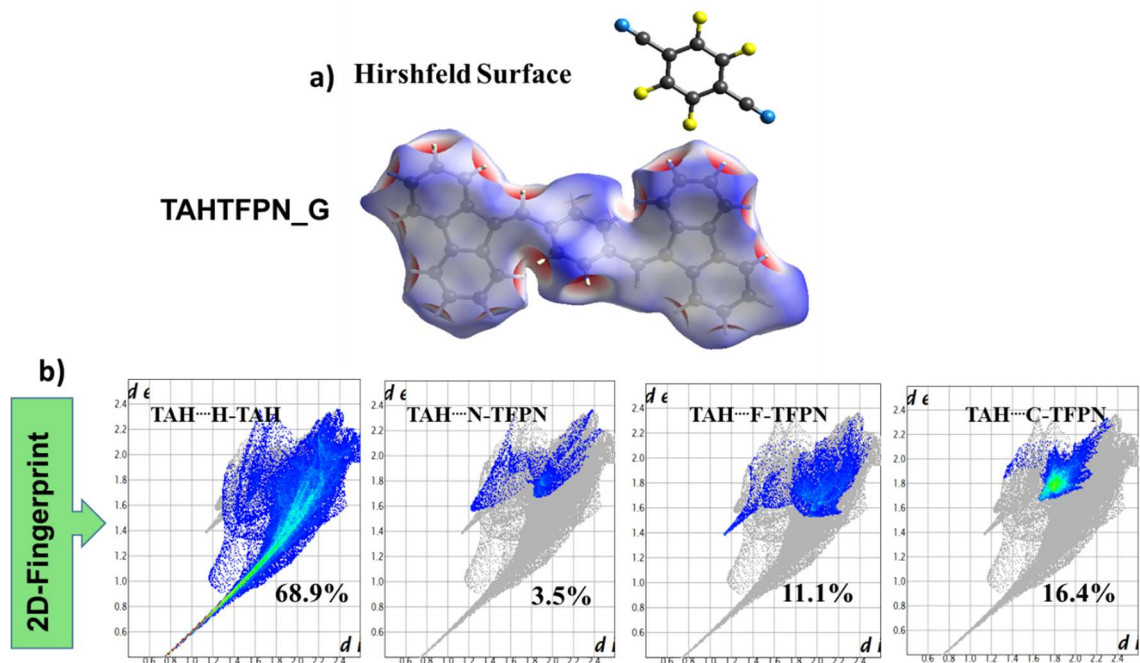
Supplementary Fig. 22: (a-d) Supramolecular rigid 3D network assembly via charge transfer interactions of (a) TAHOFN, (b) TAHTFPN_G, (c) TAHTFPN_O and (d) cis-TAHTCNB co-crystals respectively. Difference interactive orientation to the guest molecules resulted in variable conformations of TAH, revealing polymorphism features of all the afforded co-crystals.

Supplementary Table 6. SCXRD-crystal structural analysis with non-covalent interactions and dihedral angle for all the afforded co-crystals.

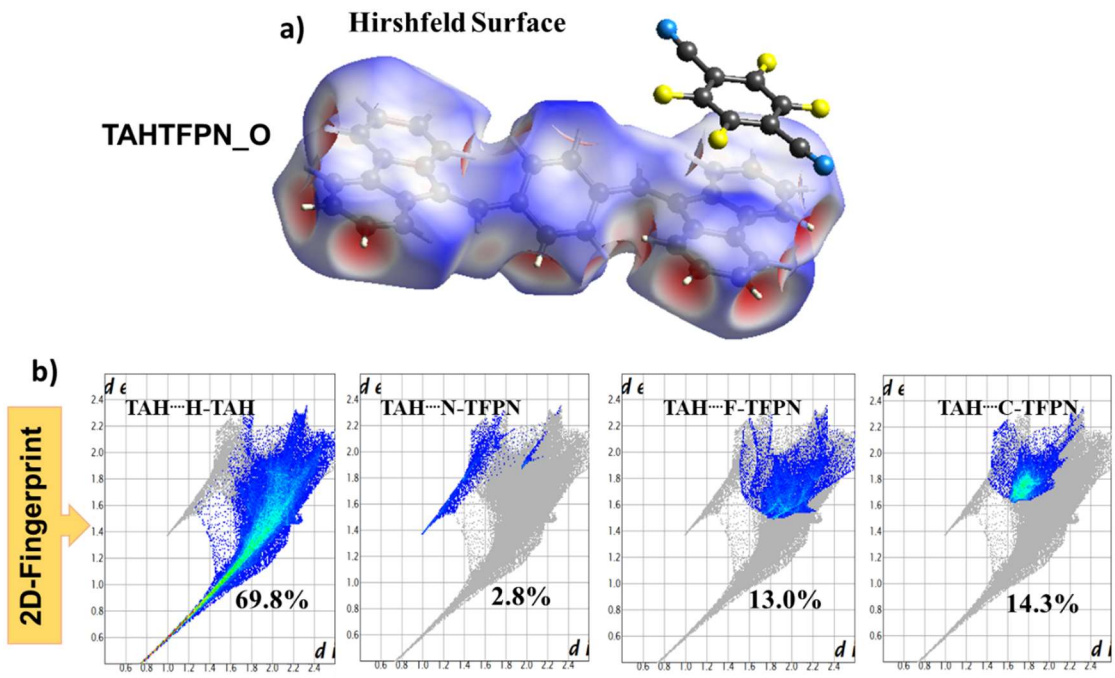
Single Crystals	<u>Inter-molecular Interactions</u>					<u>Intramolecular Interactions</u>			<u>Dihedral Angle</u>	
	<u>Close contact distance (Å)</u>					<u>Close contact distance (Å)</u>			<u>(Degree)</u>	
	CH-F	CH-N	CH- π	D-A π - π	D-D π - π	F-F	CH-N	CH- π	Inter D-A	Intra In TAH
TAHOFN	2.54	-	-	3.40	6.96	2.56	2.663	2.37 2.83	88.7	50.10
TAHTFPN_G	-	2.35	2.39	3.54	7.07	-	-	2.74 2.81	80.10	40.92
TAHTFPN_O	2.60	2.58	3.37	3.65	6.77	-	-	2.55 2.72	76.91	39.30
TAHTCNB	-	2.59	3.38	3.73	7.47	-	-	2.82 2.83	76.03	46.10



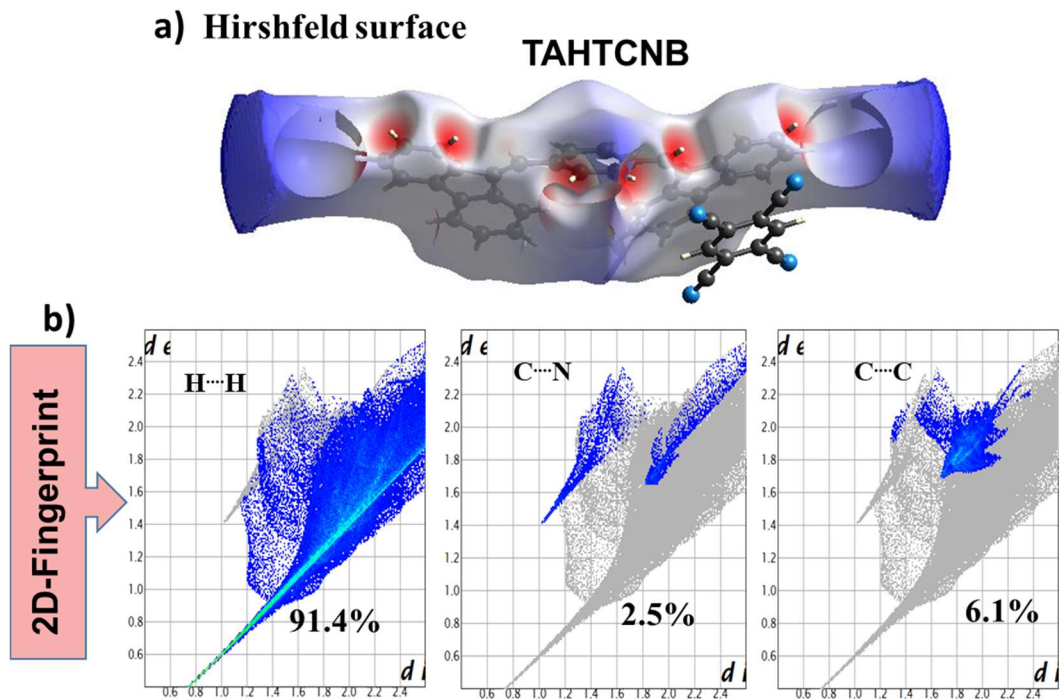
Supplementary Fig. 23: a) Hirshfeld surface images of TAHOFN co-crystal (major surface mapped on TAH). b) 2D Finger print for surface to atom intermolecular interactions mapped on Hirshfeld surface in TAHOFN.^{2,3}



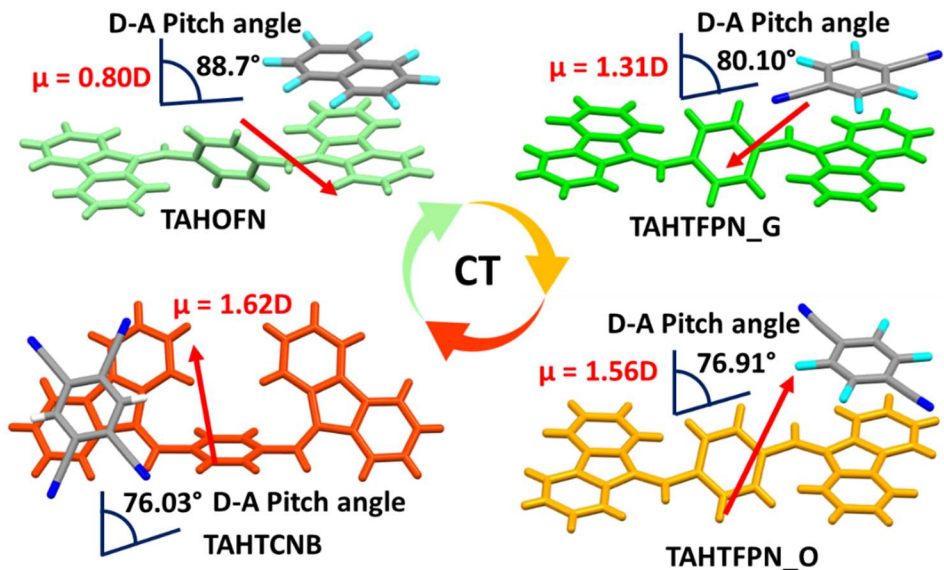
Supplementary Fig. 24: a) Hirshfeld surface images of TAHTFPN_G co-crystal (major surface mapped on TAH). b) 2D Finger print for surface to atom intermolecular interactions mapped on Hirshfeld surface in TAHTFPN_G.^{2,3}



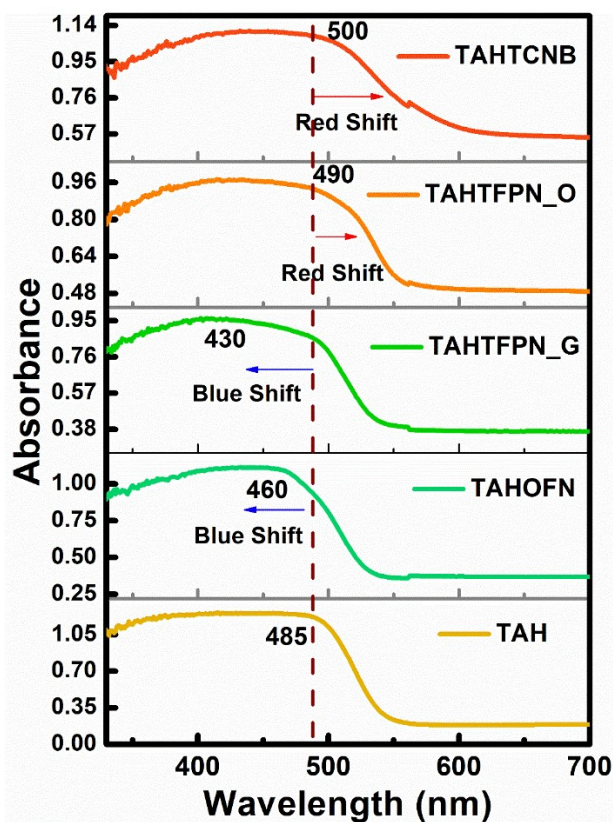
Supplementary Fig. 25: a) Hirshfeld surface images of TAHTFPN_O co-crystal (major surface mapped on TAH). b) 2D Finger print for surface to atom intermolecular interactions mapped on Hirshfeld surface in TAHTFPN_O.^{2,3}



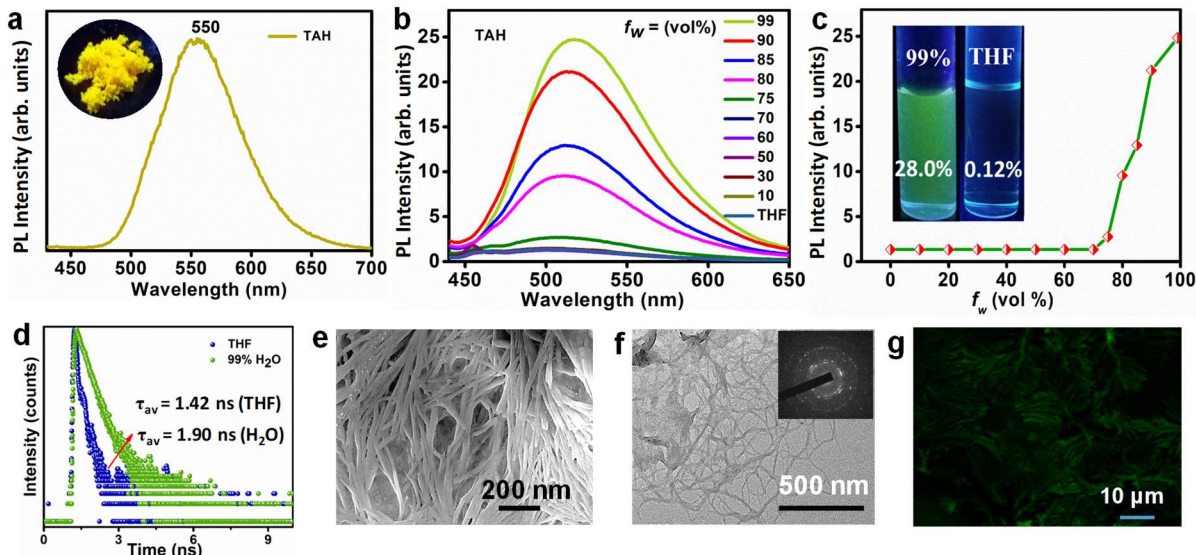
Supplementary Fig. 26: a) Hirshfeld surface images of TAHTCNB co-crystal (major surface mapped on TAH). b) 2D Finger print for surface to atom intermolecular interactions mapped on Hirshfeld surface in TAHTCNB.^{2,3}



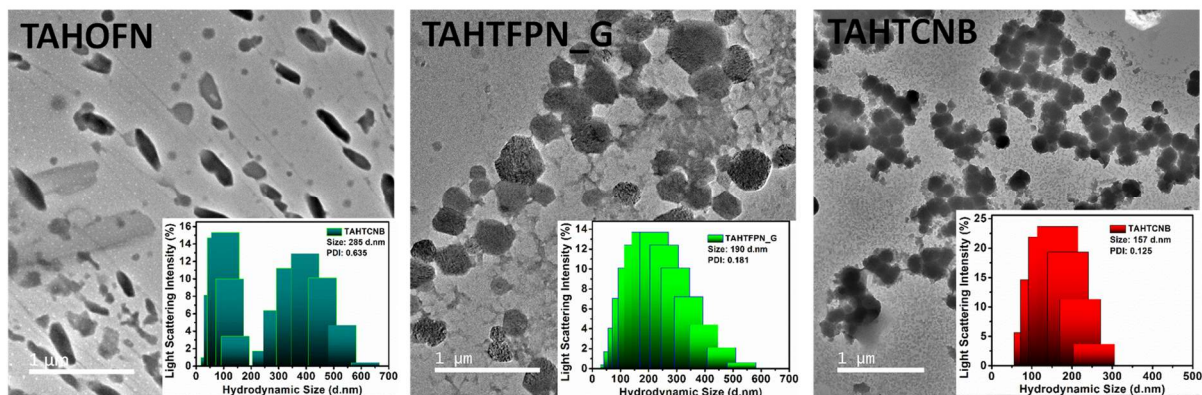
Supplementary Fig. 27: Orientation of dipole moment (μ) and pitch angles between D-A obtained from TD-DFT and SC-XRD structures of TAHOFN, TAHTFPN_G, TAHTFPN_O and TAHTCNB.



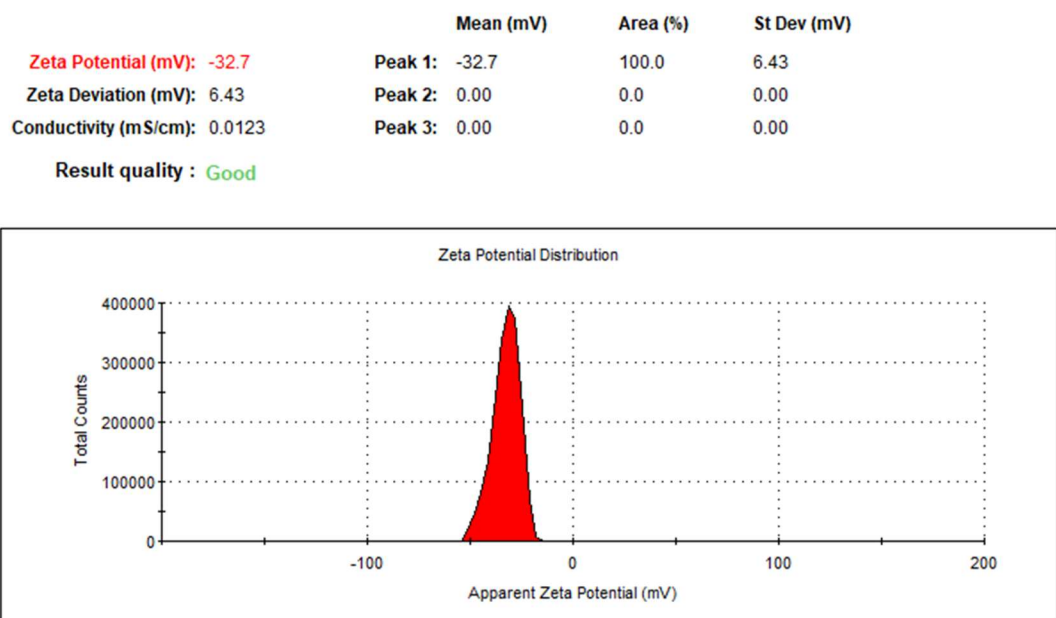
Supplementary Fig. 28: Diffuse reflection absorption spectra of TAH (yellow line), TAHOFN (off green line), TAHTFPN_G (green line), TAHTFPN_O (orange line) and TAHTCNB (red line). The absorption spectra at condensed state of the luminogens exhibited single broad absorption band in water at 400 nm and in THF at 364 nm (d).



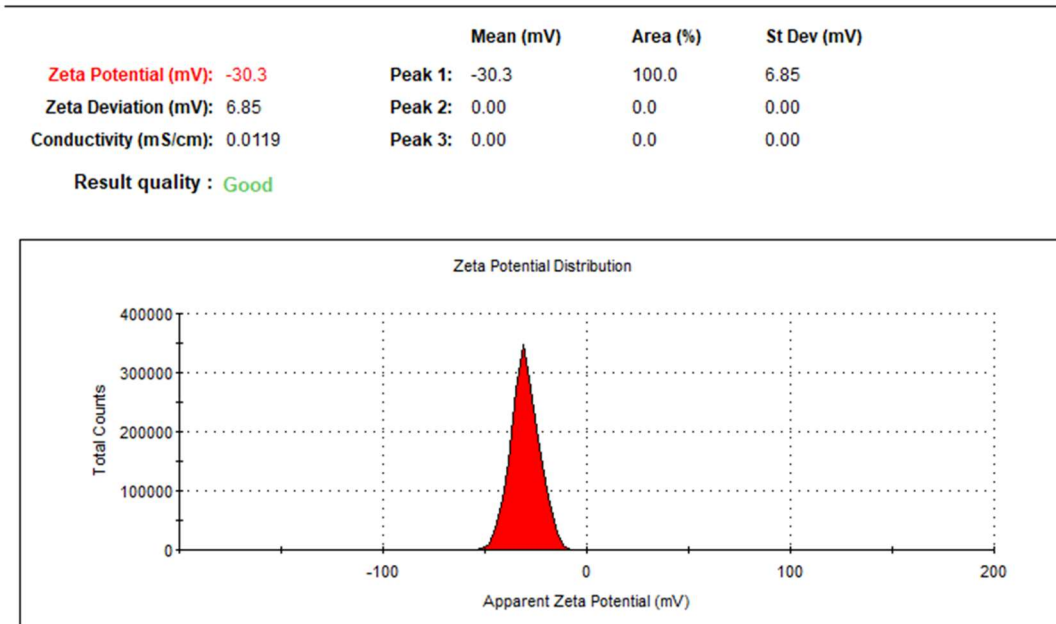
Supplementary Fig. 29: Photophysical morphological characterization of TAH: (a) Photoluminescence spectra for solid pristine TAH. (b) Aggregation-induced emission at different fractions of THF and water. (c) Relative intensity at various fractions of THF/water (inset aggregation images taken under 365 nm UV lamp and absolute PLQY). (d) TRPL decay in THF and water. (e-g) FESEM, FETEM and fluorescence images of TAH nano-ribbons formed in water. (Adapted with permission from ref 42 cited in the main MS @Copyright 2021 American Chemical Society).



Supplementary Fig. 30: FETEM images (inset: DLS graph for size distribution) of co-crystal nano aggregates formed in DMSO/H₂O (99%, f_w) for TAHOFN, TAHTFPN_G and TAHTCNB.

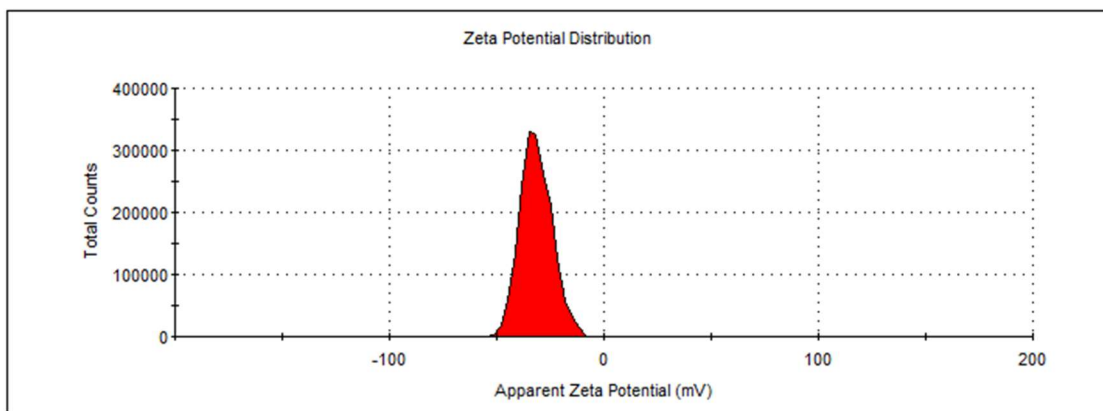


Supplementary Fig. 31: Zeta-potential recorded in H₂O for TAHOFN at 10⁻⁵ M concentration.

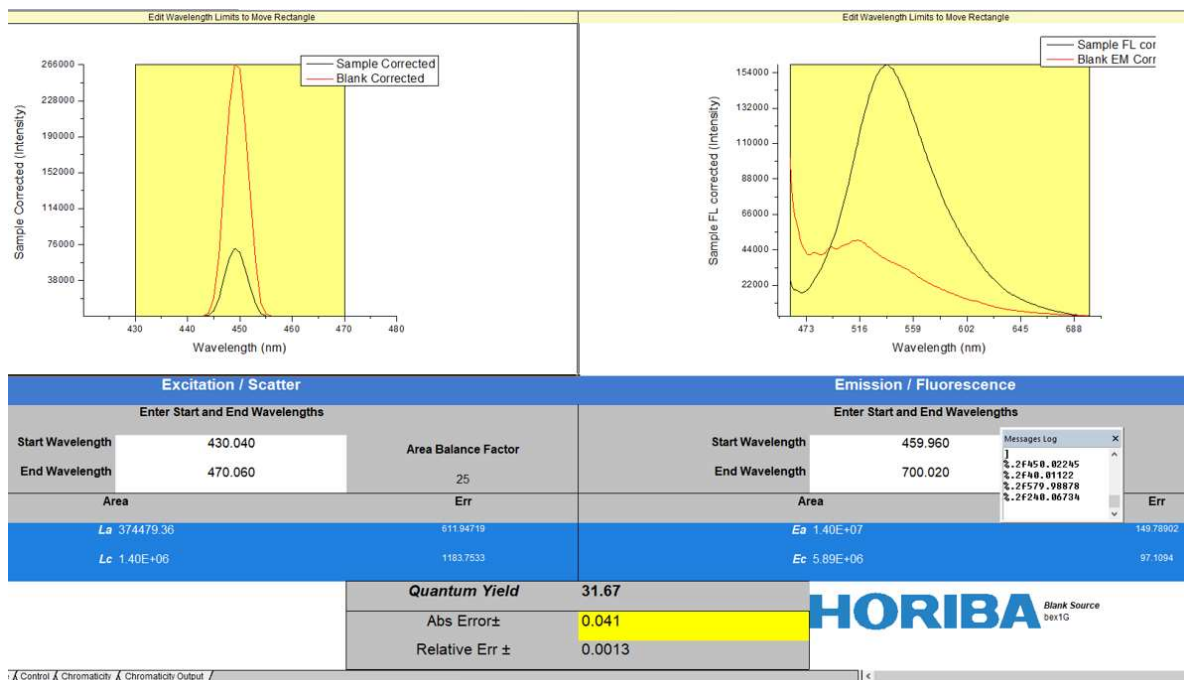


Supplementary Fig. 32: Zeta-potential recorded in H₂O for TAHTFPN_G at 10⁻⁵ M concentration.

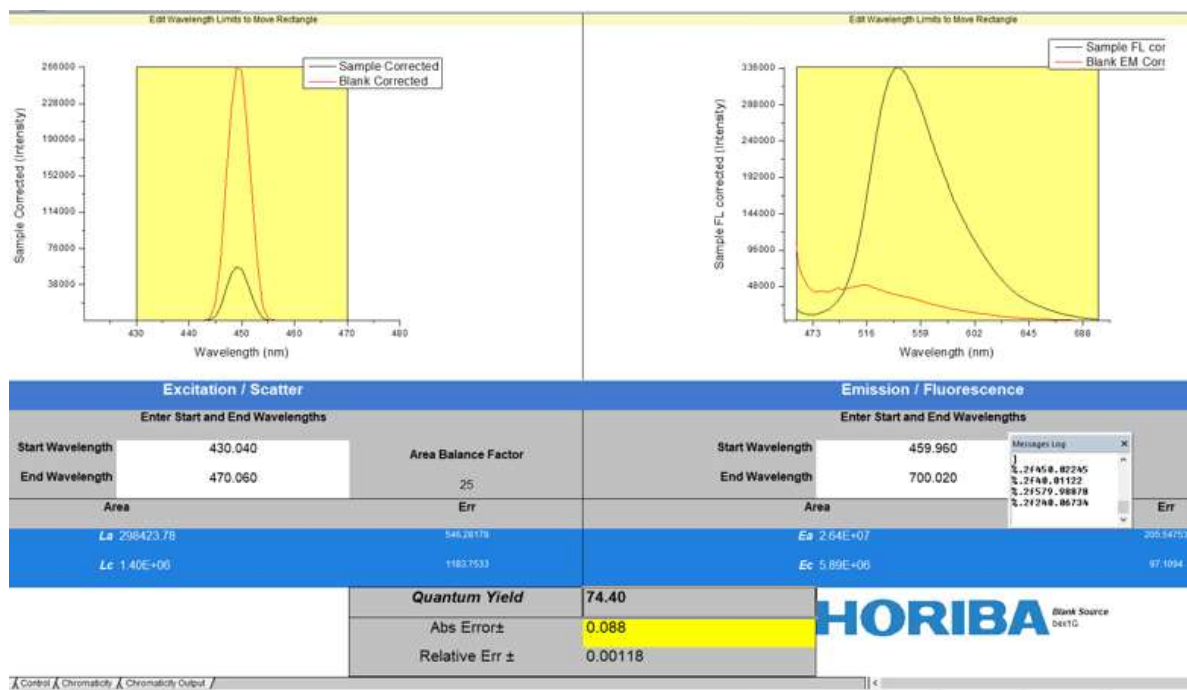
	Mean (mV)	Area (%)	St Dev (mV)
Zeta Potential (mV): -31.6	Peak 1: -31.6	100.0	7.23
Zeta Deviation (mV): 7.23	Peak 2: 0.00	0.0	0.00
Conductivity (mS/cm): 0.0103	Peak 3: 0.00	0.0	0.00
Result quality : Good			



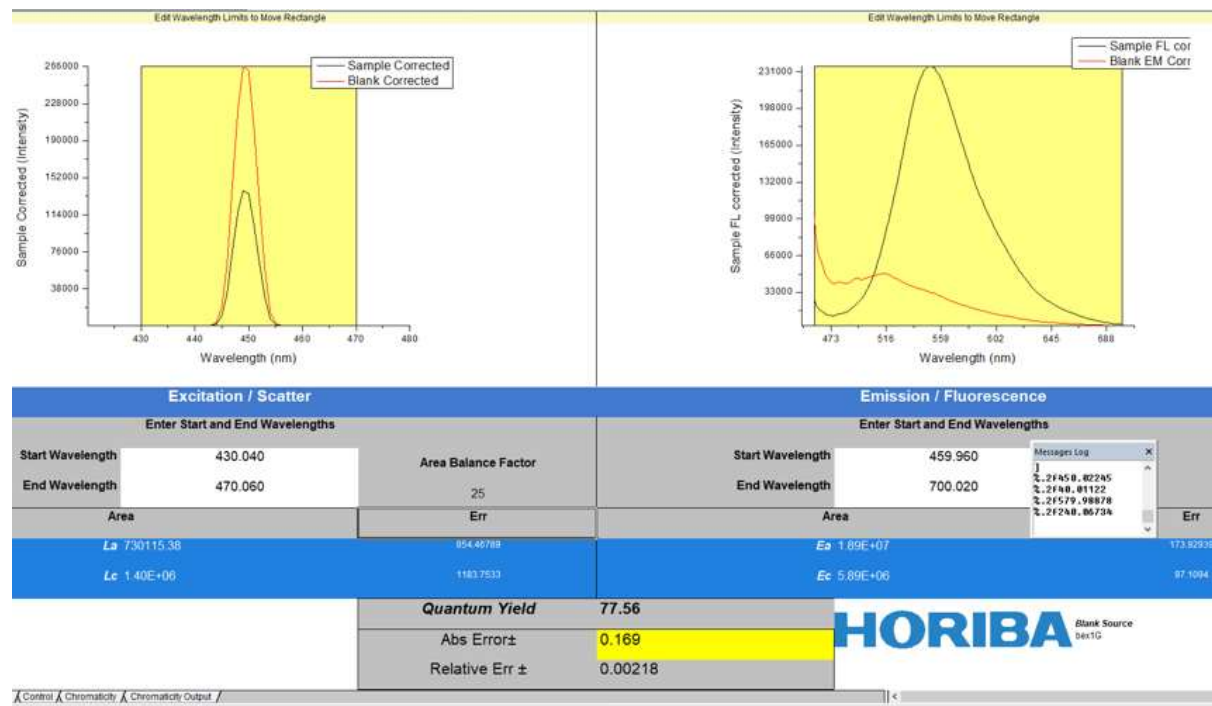
Supplementary Fig. 33: Zeta-potential recorded in H₂O for TAHTCNB at 10⁻⁵ M concentration.



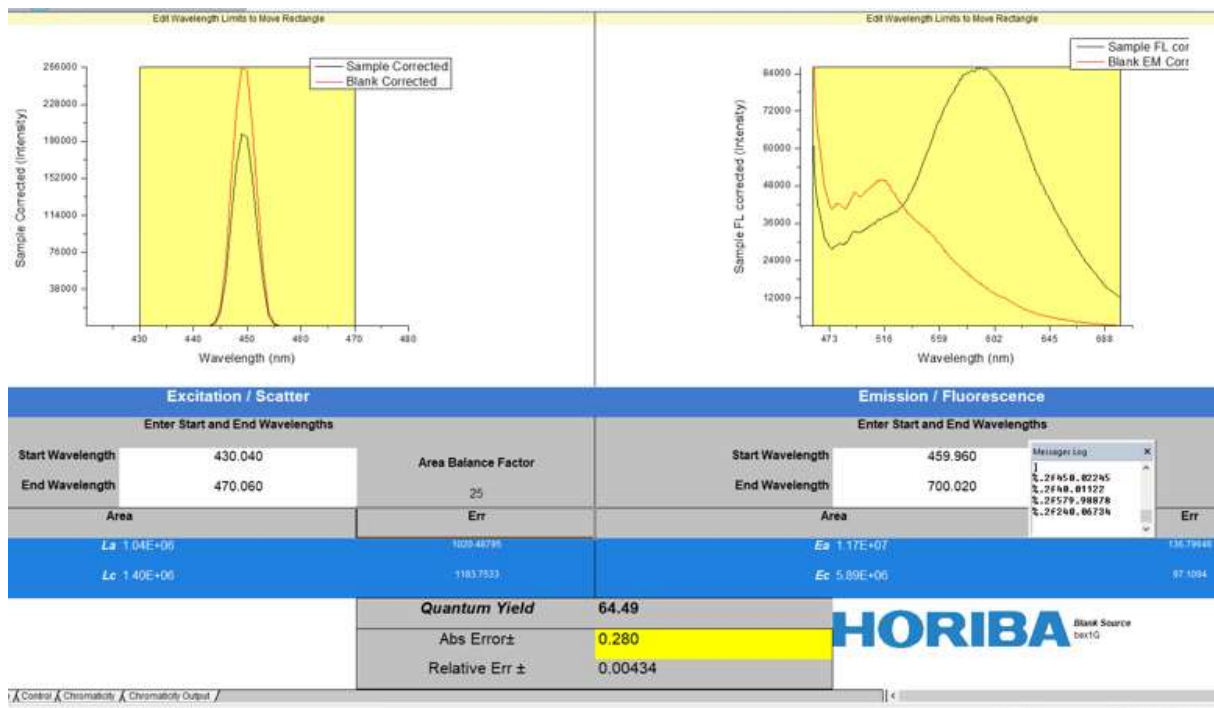
Supplementary Fig. 34: PLQY of TAHOFN co-crystal in solid state measured in the absolute method using integrating sphere.



Supplementary Fig. 35: PLQY of TAHTFPN_G co-crystal in solid state measured in the absolute method using integrating sphere.



Supplementary Fig. 36: PLQY of TAHTFPN_O co-crystal in solid state measured in the absolute method using integrating sphere.



Supplementary Fig. 37: PLQY of TAHTCNB co-crystal in solid state measured in the absolute method using integrating sphere.

Supplementary Table 7. Time resolved PL Decay of TAHOFN co-crystal Ex. 405 nm and Em. 540 nm.

❖ Exponential Components Analysis (Reconvolution)

Fitting range : [112; 510] channels

χ^2 : 0.997

	B _i	ΔB_i	f _i (%)	Δf_i (%)	τ_i (ns)	$\Delta \tau_i$ (ns)
1	0.1570	0.0018	100.000	3.524	0.505	0.012

Shift : 0.307 ns (± 0.419 ns)

Decay Background : 1.142 (± 0.139)

IRF background : 0

Supplementary Table 8. Time resolved PL Decay of TAHTFPN_G co-crystal Ex. 405 nm and Em. 545 nm.

❖ Exponential Components Analysis (Reconvolution)

Fitting range : [112; 640] channels

χ^2 : 1.009

	B_i	ΔB_i	$f_i (\%)$	$\Delta f_i (\%)$	$\tau_i (\text{ns})$	$\Delta \tau_i (\text{ns})$
1	0.1347	0.0015	100.000	1.574	0.967	0.004

Shift : 0.236 ns (± 0.643 ns)

Decay Background : 1.096 (± 0.139)

IRF background : 0

Supplementary Table 9. Time resolved PL Decay of TAHTFPN_O co-crystal Ex. 405 nm and Em. 560 nm.

❖ Exponential Components Analysis (Reconvolution)

Fitting range : [113; 1500] channels

χ^2 : 1.003

	B_i	ΔB_i	$f_i (\%)$	$\Delta f_i (\%)$	$\tau_i (\text{ns})$	$\Delta \tau_i (\text{ns})$
1	0.1388	0.0022	100.000	1.876	1.064	0.003

Shift : 0.122 ns (± 0.873 ns)

Decay Background : 1.023 (± 0.062)

IRF background : 0

Supplementary Table 10. Time resolved PL Decay of TAHTCNB co-crystal Ex. 405 nm and Em. 590 nm.

❖ Exponential Components Analysis (Reconvolution)

Fitting range : [113; 3900] channels

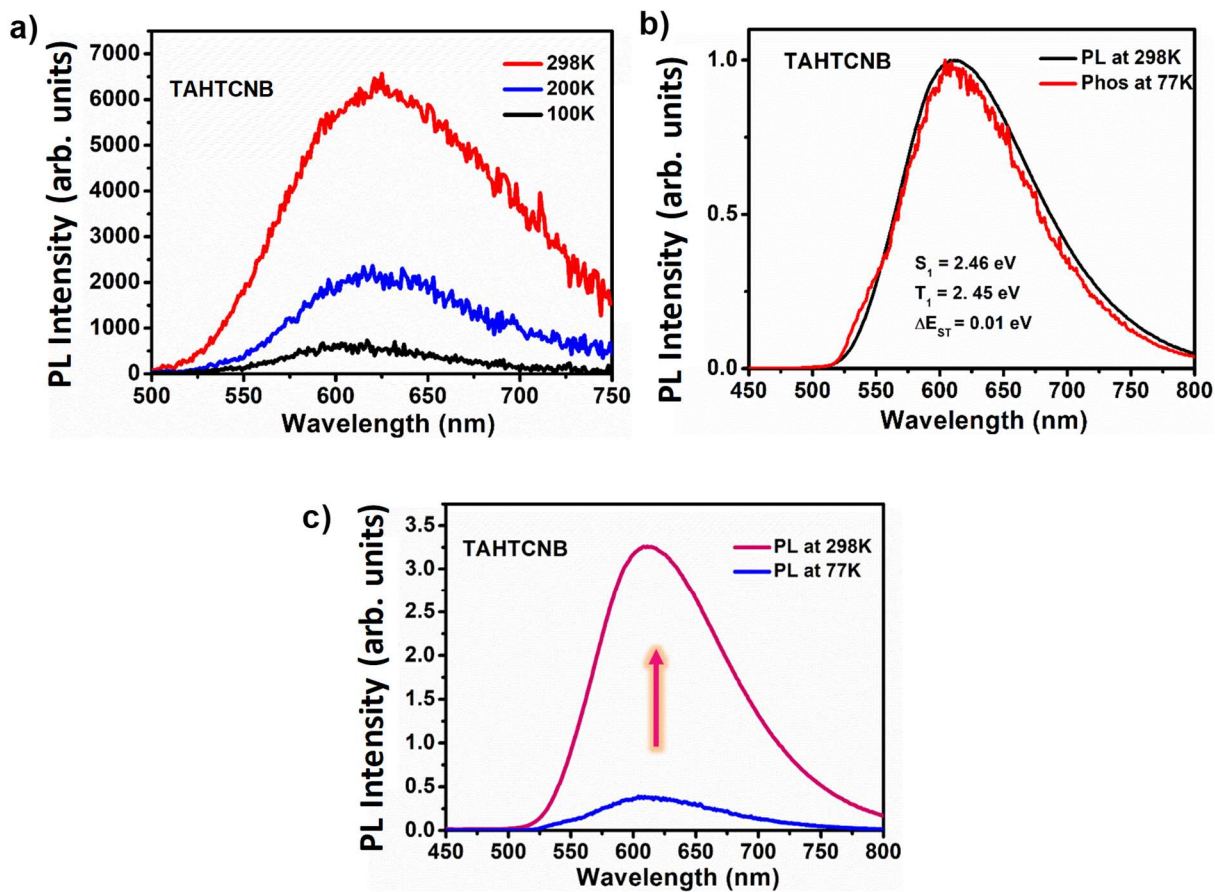
χ^2 : 1.034

	B_i	ΔB_i	$f_i (\%)$	$\Delta f_i (\%)$	$\tau_i (\text{ns})$	$\Delta \tau_i (\text{ns})$
1	0.0763	0.0052	2.970	0.858	0.570	0.126
2	0.0115	0.0006	4.142	0.229	5.253	0.018
3	0.0433	0.0004	92.888	0.830	31.432	0.0004

Shift : 0.098 ns (± 3.634 ns)

Decay Background : 8.010 (± 1.265)

IRF background : 0



Supplementary Fig. 38: a) Temperature dependent delayed emission spectra for TAHTCNB co-crystal in solid state. b) PL at RT and phosphorescence at 77K. c) Steady state PL at RT and 77K for TAHTCNB solid state (powder).

Supplementary Table 11. Fitting results for delayed decay at 300K for TAHTCNB co-crystal.

Fit Range (ch) : 185 to 3999

Parameter	Value	Std. Dev.	Rel %
τ_1	8.962E-007 s	6.0113E-009 s	
τ_2	9.491E-006 s	4.8427E-008 s	
B1	9114.886	57.2142	47.84
B2	938.583	7.7630	52.16
A	6.201		
χ^2	1.323		

Supplementary Table 12. Fitting results for delayed decay at 200K for TAHTCNB co-crystal.

Fit Range (ch) : 182 to 3999

<u>Parameter</u>	<u>Value</u>	<u>Std. Dev.</u>	<u>Rel %</u>
τ_1	1.096E-006 s	6.1522E-009 s	
τ_2	9.409E-006 s	3.6525E-008 s	
B1	10989.283	55.5040	49.77
B2	1291.460	9.3091	50.23
A	0.537		
χ^2	1.109		

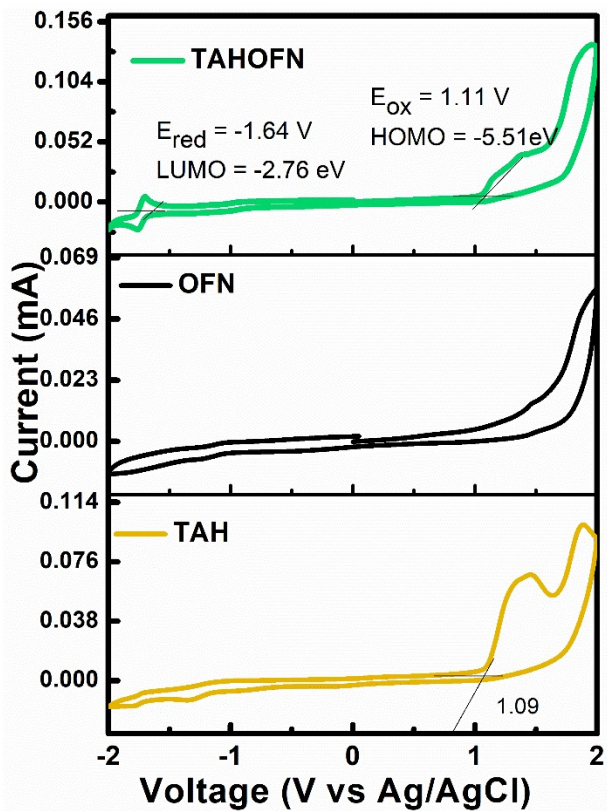
Supplementary Table 13. Fitting results for delayed decay at 100K for TAHTCNB co-crystal.

Fit Range (ch) : 182 to 3999

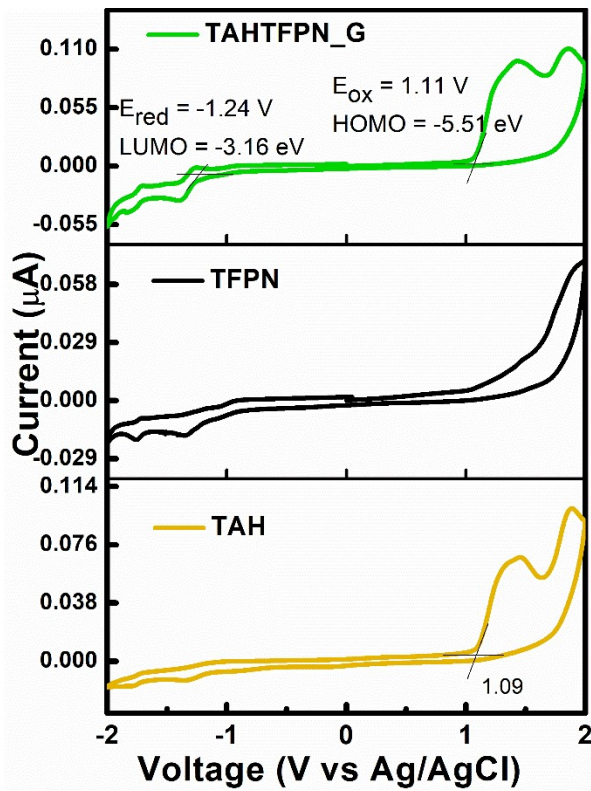
<u>Parameter</u>	<u>Value</u>	<u>Std. Dev.</u>	<u>Rel %</u>
τ_1	1.012E-006 s	5.5946E-009 s	
τ_2	9.728E-006 s	4.3891E-008 s	
B1	10797.647	56.6338	53.67
B2	969.972	7.7391	46.33
A	1.118		
χ^2	1.102		

Supplementary methods for Electrochemical properties

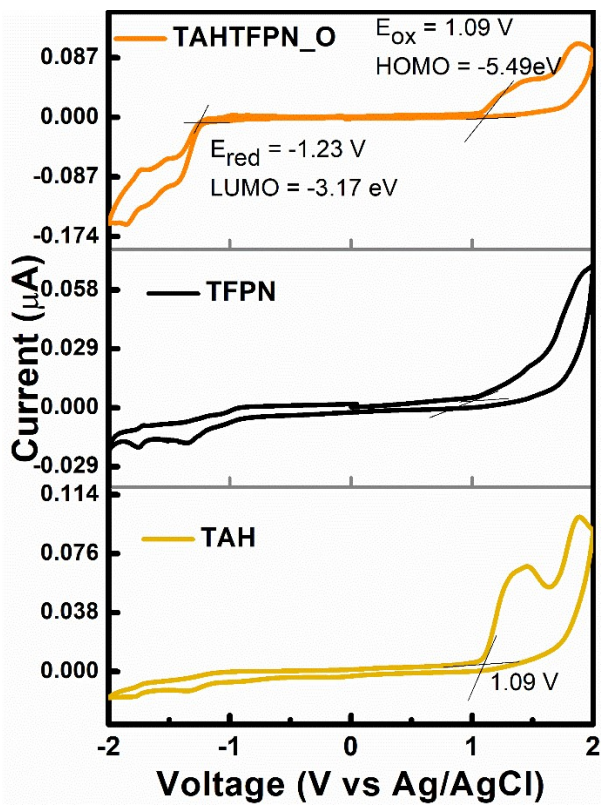
To predict the HOMO and LUMO energy levels, the cyclic voltammetry (CV) studies were performed at room temperature by drop casting the luminogens on the working electrodes from THF solution. Supplementary Fig. 39-42 explains the CV curves and the onset values that are obtained and the corresponding energy levels are tabulated in Supplementary Table S14. Both the luminogens displayed only oxidation curves and by substituting the onset values of oxidation into $E_{\text{HOMO}} = -[(E_{\text{ox}} - E_{1/2} \text{ (ferrocene)}) + 4.8 \text{ eV}]$ the HOMO energy levels were obtained. The LUMO of the monomers were estimated from $E_{\text{HOMO}} = -[(E_{\text{ox}} - E_{1/2} \text{ (ferrocene)}) - 4.8 \text{ eV}]$.



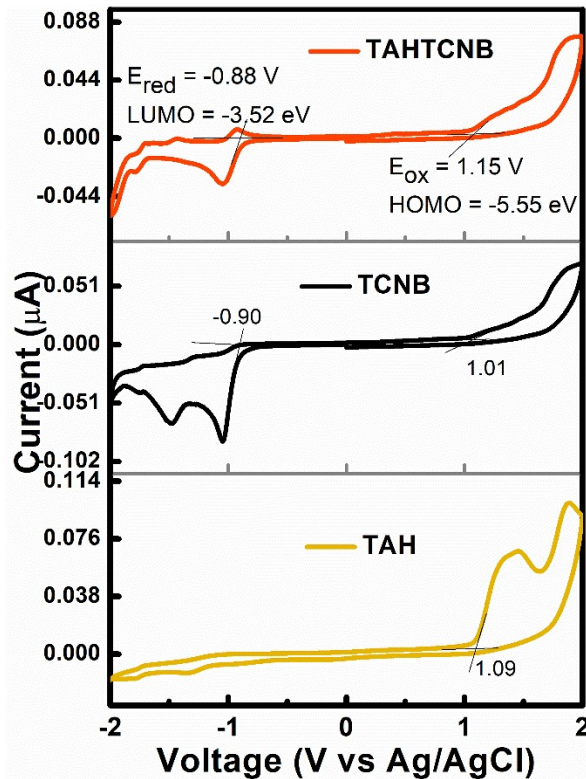
Supplementary Fig. 39: Cyclic voltammetry (CV) curves of TAH crystals (yellow line), OFN (black line) and TAHOFN (off-green line).



Supplementary Fig. 40: Cyclic voltammetry (CV) curves of TAH crystals (yellow line), TFPN (black line) and TAHTFPN_G (green line).



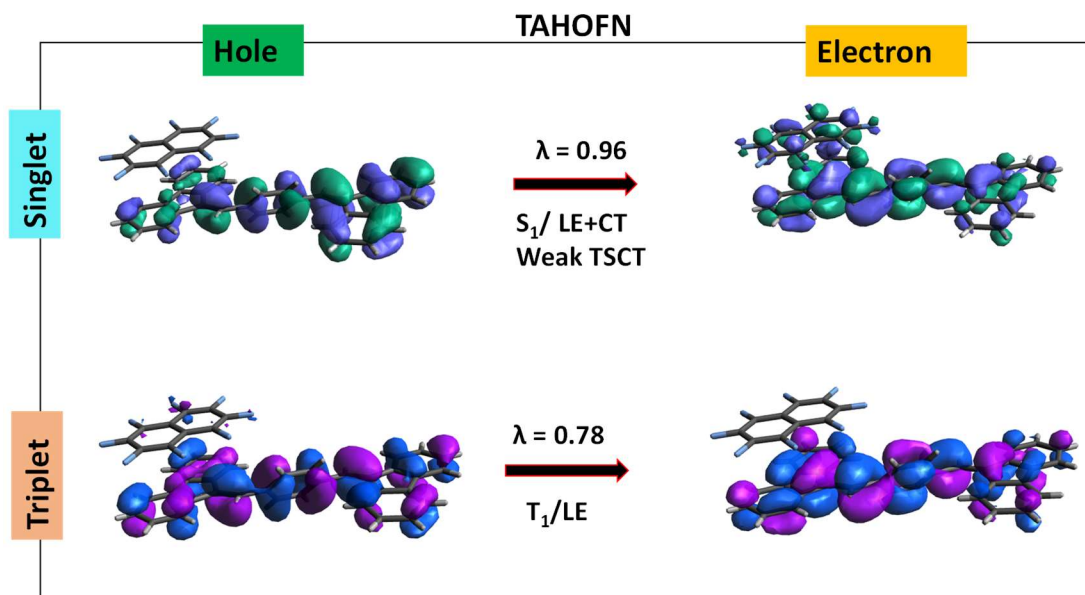
Supplementary Fig. 41: Cyclic voltammetry (CV) curves of TAH crystals (yellow line), TFPN (black line) and TAHTFPN_O (orange line).



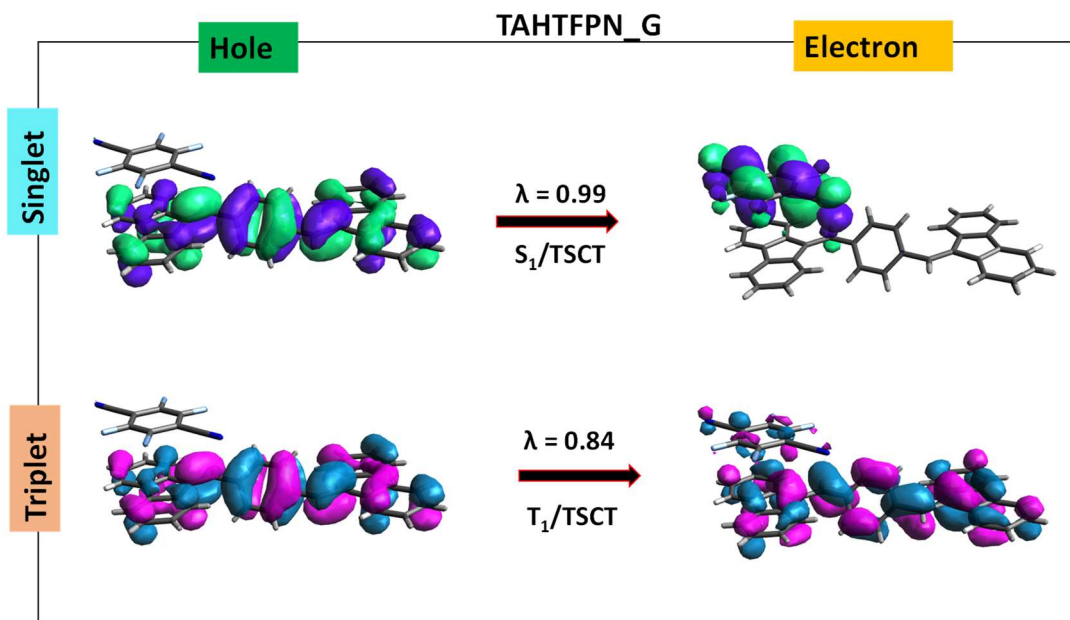
Supplementary Fig. 42: Cyclic voltammetry (CV) curves of TAH crystals (yellow line), TCNB (black line) and TAHTCNB (red line).

Supplementary Table S14. The energy levels calculated from cyclic voltammetry and DFT.

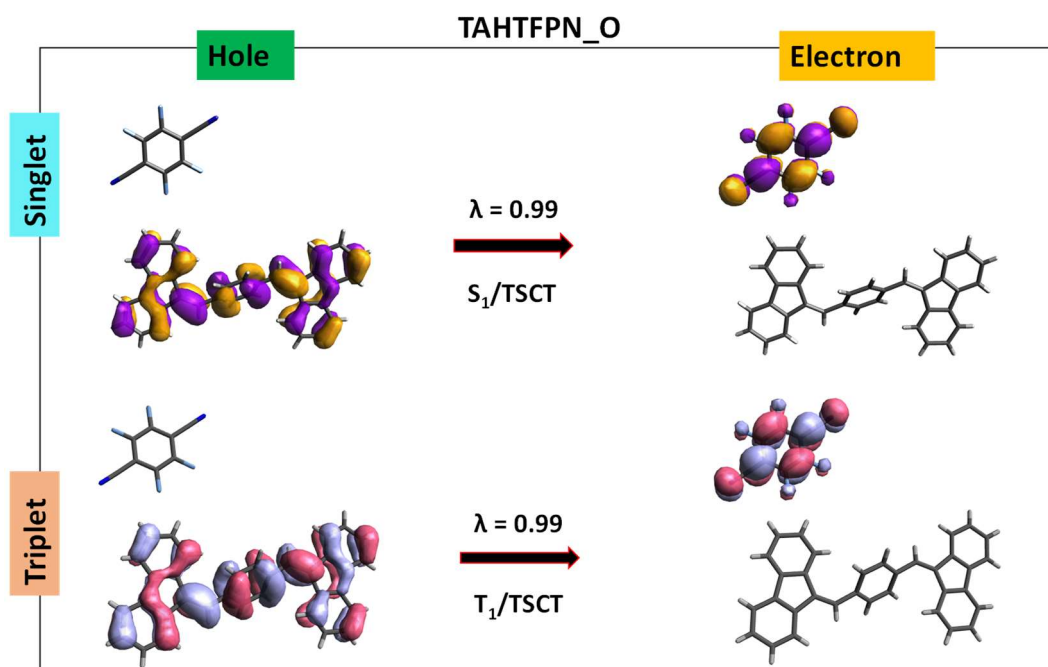
Compound	Experimental data					DFT data (eV)			
	E _{ox} /V	E _{red} /V	E _{HOMO} /eV	E _{LUMO} /eV	E _{opt} /eV	H-L Gap/eV	HOMO	LUMO	H-L Gap
TAH	1.09	-	-5.49	-2.96	2.53	2.53	-5.47	-2.17	3.29
TAHOFN	1.11	-1.64	-5.51	-2.76	-	2.75	-5.51	-2.76	2.75
TAHTFPN	1.11	-1.24	-5.51	-3.16	-	2.35	-5.58	-2.69	2.89
_G									
TAHTFPN	1.09	-1.23	-5.49	-3.17	-	2.32	-5.48	-2.80	2.68
_O									
TAHTCNB	1.15	-0.88	-5.55	-3.52	-	2.03	-5.55	-3.52	2.033



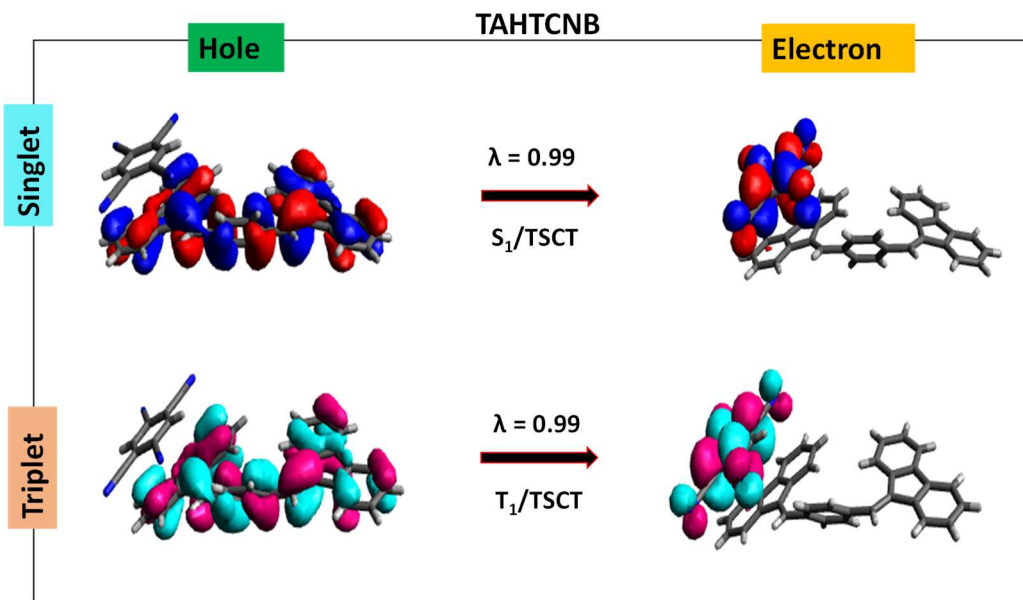
Supplementary Fig. 43: Natural transition orbitals (NTOs)⁴ for lowest excited singlet and triplet excited states in TAHOFN.



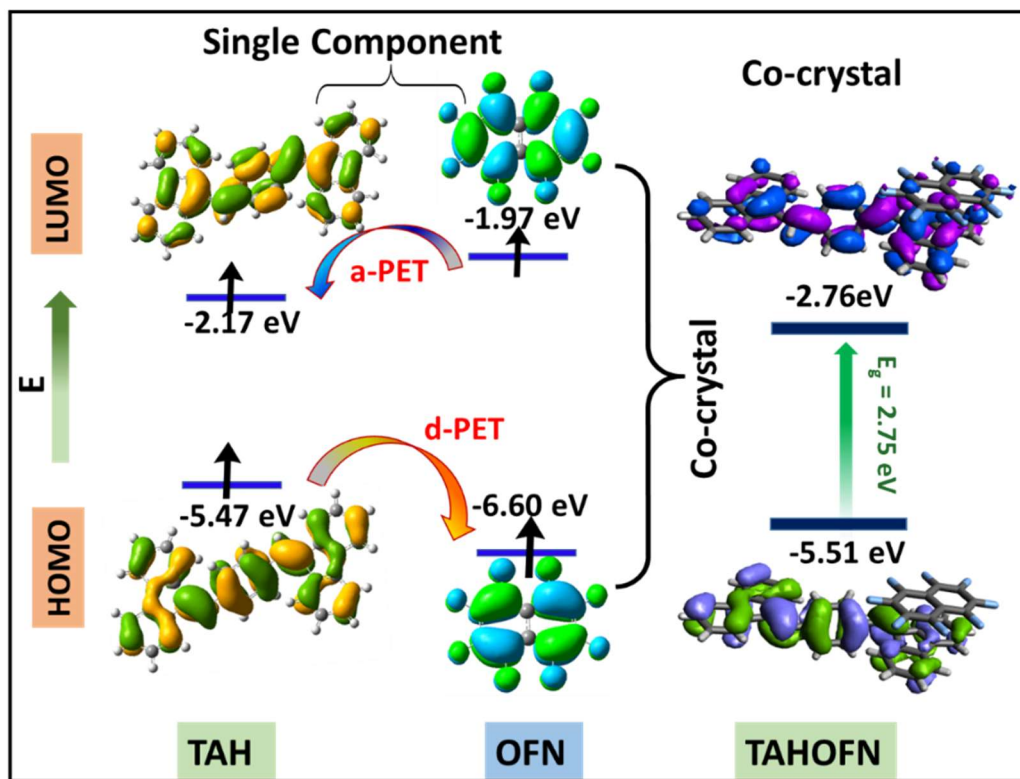
Supplementary Fig. 44: Natural transition orbitals (NTOs)⁴ for lowest excited singlet and triplet excited states in TAHTFPN_G.



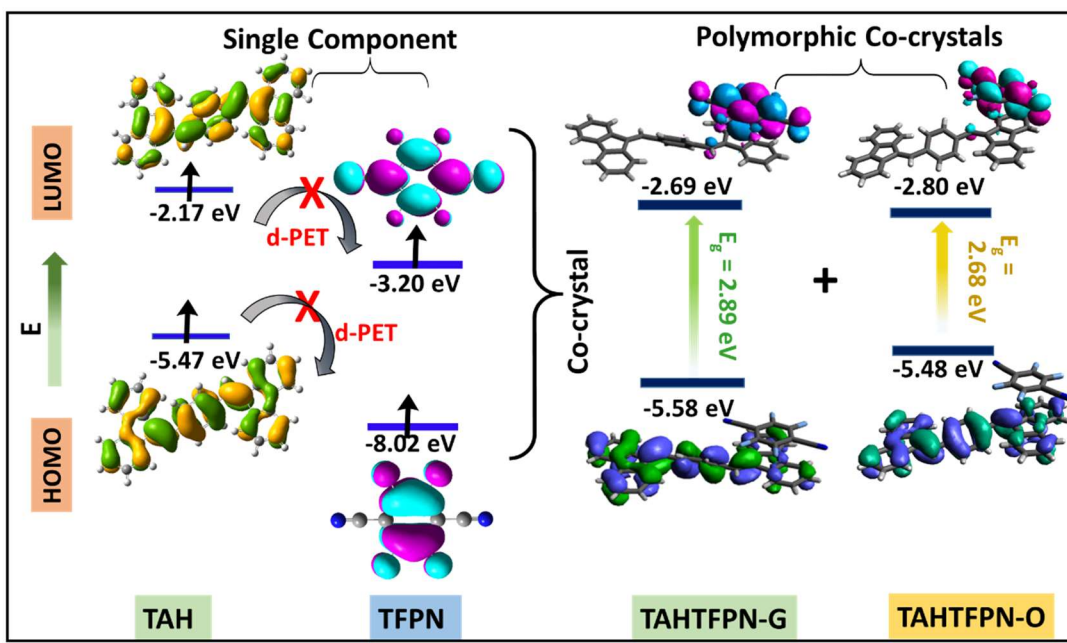
Supplementary Fig. 45: Natural transition orbitals (NTOs)⁴ for lowest excited singlet and triplet excited states in TAHTFPN_O.



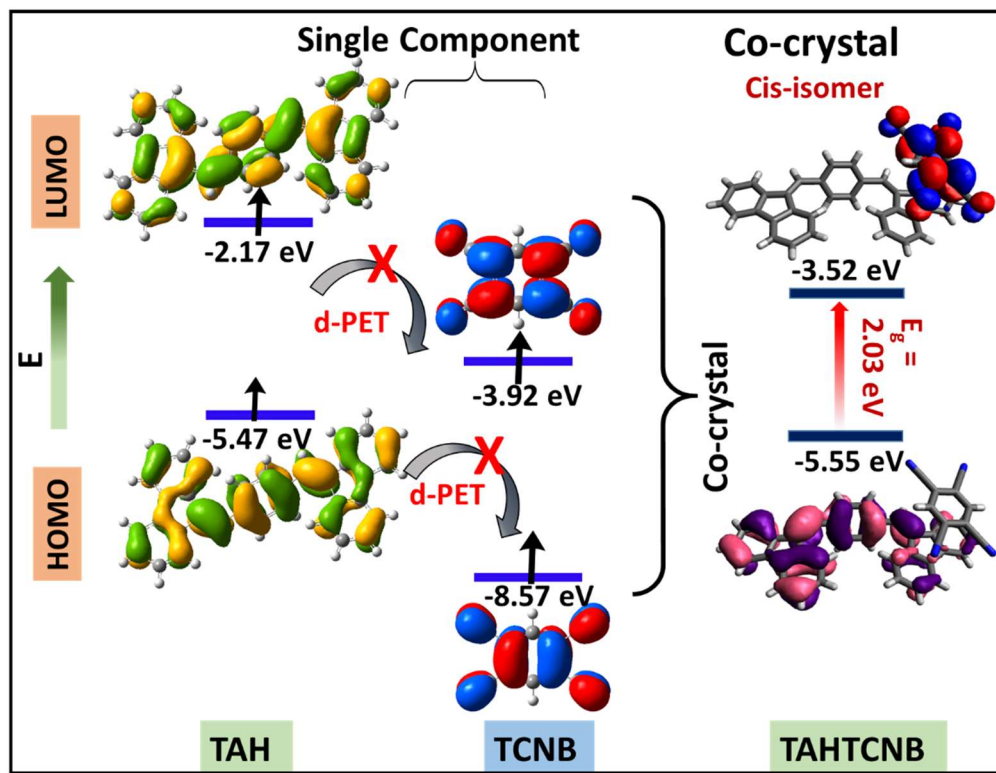
Supplementary Fig. 46: Natural transition orbitals (NTOs)⁴ for lowest excited singlet and triplet excited states in TAHTCNB.



Supplementary Fig. 47: Mechanism of weak fluorescence (a-PET & d-PET) for TAHOFN by DFT/TD-DFT⁴ calculated HOMO/LUMO energy band diagram for conformer TAH and OFN.



Supplementary Fig. 48: Color-tunable fluorescence and CT mechanism for the polymorphic co-crystals of TAHTFPN_G and TAHTFPN_O by DFT/TD-DFT⁴ calculated HOMO/LUMO energy band diagram for the conformer TAH and TFPN.



Supplementary Fig. 49: Red fluorescence and strong narrow band CT mechanism for the cis-isomeric co-crystals of TAHTCNB by DFT/TD-DFT⁴ calculated HOMO/LUMO energy band diagram for the conformer TAH and TCNB.

Supplementary Table 15. Vertical energy transitions with major frontier orbital contribution for TAHOFN cocrystal at B3LYP/6-31G(d,p) level for singlet states⁴.

State	Energy (eV)	Energy (cm ⁻¹)	Wavelength (nm)	Osc. Strength (<i>f</i>)	Symmetry	Major contributions
S ₁	3.19	25741.18	388	0.5471	H-1→LUMO	22%
S ₂	3.21	25943.63	385	0.3236	H-1→LUMO	64%
S ₃	3.30	26652.59	375	0.0058	H-2→LUMO	93%
S ₄	3.59	29025.47	344	0.0674	H-3→LUMO	23%
S ₅	3.61	29162.59	342	0.0344	H-4→LUMO	14%
S ₆	3.71	29990.92	333	0.0564	H-4→LUMO	52%
S ₇	3.75	30253.05	330	0.0012	H-2→L+1	86%
S ₈	3.76	30356.29	329	0.0054	H-2→L+1	13%
S ₉	3.99	32217.01	310	0.0003	H-1→L+1	35%
S ₁₀	4.03	32531.57	307	0.001	H-4→LUMO	17%

Supplementary Table 16. Vertical energy transitions with major frontier orbital contribution for TAHOFN cocrystal at B3LYP/6-31G (d,p) level for triplet states⁴.

State	Energy (eV)	Energy (cm ⁻¹)	Wavelength (nm)	Osc. Strength (<i>f</i>)	Symmetry	Major contributions
T ₁	2.23	18025.68	554	0	HOMO→LUMO	72%
T ₂	2.47	19940.45	501	0	H-4→LUMO	16%
T ₃	2.65	21430.96	466	0	H-1→L+1	33%
T ₄	2.72	21985.06	454	0	H-1→LUMO	44%
T ₅	2.77	22404.47	446	0	H-2→LUMO	62%
T ₆	3.43	27675.3	361	0	H-8→LUMO	13%

T7	3.46	27953.56	357	0	H-1→LUMO	37%
T8	3.49	28214.89	354	0	H-2→LUMO	24%
T9	3.57	28827.06	346	0	HOMO→L+1	58%
T10	3.62	29209.37	342	0	H-4→LUMO	37%

Supplementary Table 17. Vertical energy transitions with major frontier orbital contribution for TAHTFPN_G cocrystal at B3LYP/6-31G(d,p) level for singlet states⁴.

State	Energy (eV)	Energy (cm ⁻¹)	Wavelength (nm)	Osc. Strength (f)	Symmetry	Major contributions
S₁	2.45	19812.20	504	0.061	HOMO→LUMO	96%
S₂	2.76	22304.45	448	0.0043	H-2→LUMO	99%
S₃	2.82	22811.77	438	0.0001	H-1→LUMO	98%
S₄	3.07	24777.35	403	0.8762	HOMO→L+1	91%
S₅	3.10	25037.06	399	0.0585	H-3→LUMO	88%
S₆	3.14	25351.61	394	0.0735	H-1→L+1	87%
S₇	3.32	26823.58	372	0.0051	H-2→L+1	95%
S₈	3.67	29618.29	337	0.1259	H-3→L+1	53%
S₉	3.69	29770.73	335	0.0049	H-5→LUMO	96%
S₁₀	3.78	30561.15	327	0.0009	H-4→LUMO	98%

Supplementary Table 18. Vertical energy transitions with major frontier orbital contribution for TAHTFPN_G cocrystal at B3LYP/6-31G (d,p) level for triplet states⁴.

State	Energy (eV)	Energy (cm ⁻¹)	Wavelength (nm)	Osc. Strength (f)	Symmetry	Major contributions
T1	2.09	16873.92	592	0	HOMO→LUMO	13%
T2	2.42	19562.97	511	0	HOMO→LUMO	57%
T3	2.51	20267.09	493	0	H-3→L+1	38%
T4	2.68	21689.86	461	0	H-1→LUMO	17%
T5	2.71	21862.46	457	0	H-2→LUMO	74%
T6	2.83	22872.27	437	0	H-2→LUMO	25%
T7	2.86	23068.26	433	0	H-1→LUMO	82%
T8	3.08	24855.58	402	0	H-3→LUMO	86%
T9	3.32	26809.86	372	0	H-11→LUMO	46%
T10	3.37	27222.01	367	0	H-11→LUMO	12%

Supplementary Table 19. Vertical energy transitions with major frontier orbital contribution for TAHTFPN_O cocrystal at B3LYP/6-31G(d,p) level for singlet states⁴.

State	Energy (eV)	Energy (cm ⁻¹)	Wavelength (nm)	Osc. Strength (f)	Symmetry	Major contributions
S1	2.26	18270.07	547	0.0445	HOMO→LUMO	96%
S2	2.57	20767.16	481	0.0157	H-2→LUMO	98%
S3	2.68	21673.73	461	0.0164	H-1→LUMO	84%
S4	2.78	22429.47	445	0.9245	HOMO→L+1	82%
S5	2.84	22967.44	435	0.2535	H-1→L+1	75%
S6	2.97	23964.35	417	0.0055	H-2→L+1	96%
S7	2.98	24103.88	414	0.0126	H-3→LUMO	94%
S8	3.37	27228.47	367	0.0558	H-3→L+1	58%

S₉	3.66	29580.38	338	0.0021	H-1→L+2	81%
S₁₀	3.67	29649.75	337	0.0045	H-5→LUMO	91%

Supplementary Table 20. Vertical energy transitions with major frontier orbital contribution for TAHTFPN_O cocrystal at B3LYP/6-31G (d,p) level for triplet states⁴.

State	Energy (eV)	Energy (cm ⁻¹)	Wavelength (nm)	Osc. Strength (<i>f</i>)	Symmetry	Major contributions
T₁	1.72	13934.84	717	0	HOMO→L+1	77%
T₂	2.17	17575.63	568	0	H-3→L+1	35%
T₃	2.28	18464.45	541	0	H-3→L+1	12%
T₄	2.42	19558.94	511	0	H-1→L+1	60%
T₅	2.47	19937.22	501	0	H-2→LUMO	57%
T₆	2.57	20778.46	481	0	H-2→LUMO	40%
T₇	2.72	22003.61	454	0	H-1→LUMO	91%
T₈	2.97	23986.12	416	0	H-3→LUMO	88%
T₉	3.24	26138.82	382	0	H-3→L+1	27%
T₁₀	3.27	26436.43	378	0	H-11→LUMO	54%

Supplementary Table 21. Vertical energy transitions with major frontier orbital contribution for TAHTCNB cocrystal at B3LYP/6-31G(d,p) level for singlet states⁴.

State	Energy (eV)	Energy (cm ⁻¹)	Wavelength (nm)	Osc. Strength (<i>f</i>)	Symmetry	Major contributions
S₁	1.95	15740.72	635	0.0047	HOMO→LUMO	93%
S₂	2.19	17703.87	564	0.0174	H-2→LUMO	80%
S₃	2.20	17759.52	563	0.0049	H-2→LUMO	19%

S₄	2.47	19933.99	501	0.0078	H-3→LUMO	92%
S₅	2.62	21180.93	472	0.0293	HOMO→L+1	92%
S₆	2.83	22868.24	437	0.0005	H-2→L+1	99%
S₇	2.88	23253.77	430	0.00	H-1→L+1	98%
S₈	3.10	25066.1	398	0.0012	H-6→LUMO	25%
S₉	3.14	25360.49	394	0.0289	H-3→L+1	84%
S₁₀	3.17	25627.46	390	0.0005	H-6→LUMO	13%

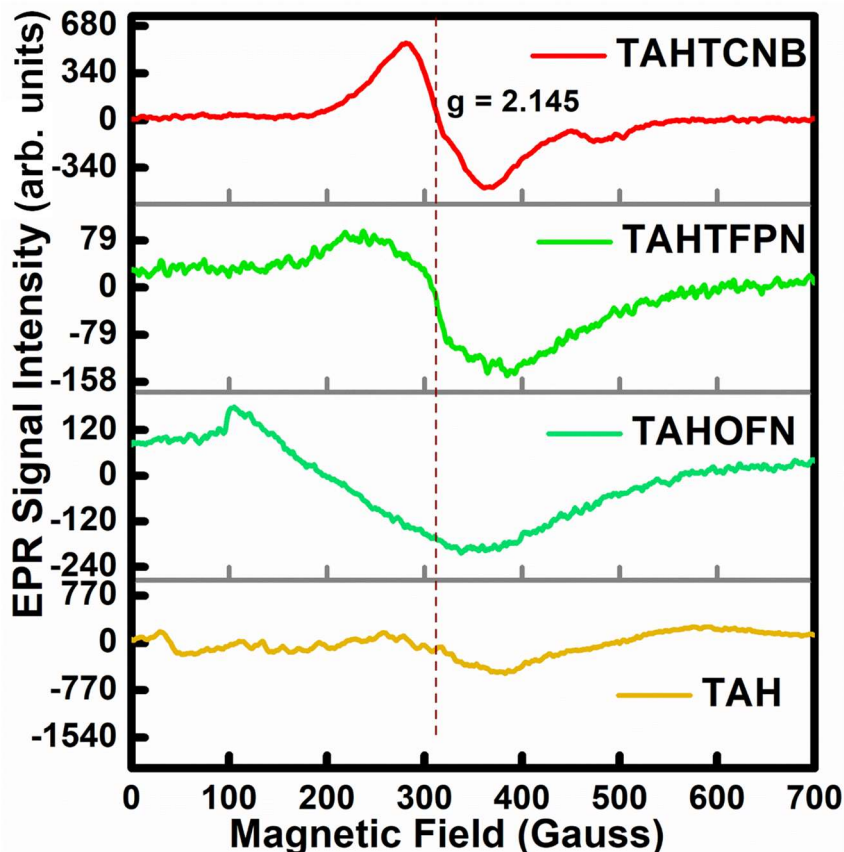
Supplementary Table 22. Vertical energy transitions with major frontier orbital contribution for TAHTCNB cocrystal at B3LYP/6-31G (d,p) level for triplet states⁴.

State	Energy (eV)	Energy (cm ⁻¹)	Wavelength (nm)	Osc. Strength (f)	Symmetry	Major contributions
T1	1.93	15599.57	641	0	HOMO→LUMO	91%
T2	2.13	17233.65	580	0	H-2→LUMO	99%
T3	2.20	17748.23	563	0	H-1→LUMO	98%
T4	2.23	18033.75	554	0	H-3→L+3	10%
T5	2.45	19787.2	505	0	H-3→LUMO	89%
T6	2.48	20079.17	498	0	H-3→L+2	35%
T7	2.64	21342.24	468	0	H-3→L+2	10%
T8	2.73	22033.45	453	0	H-1→L+2	38%
T9	2.74	22157.66	451	0	H-2→L+1	56%
T10	2.89	23311.04	428	0	H-10→LUMO	12%

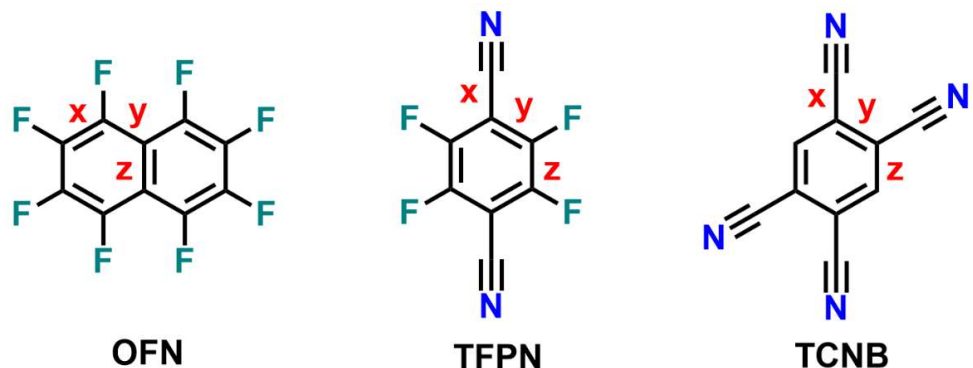
Supplementary Table 23. SOC-matrix element (SOCME) calculated by using ORCA 4.5.0 software with ORCA_SOC module⁵.

	SOCME_TAHOFN (cm ⁻¹)		SOCME_TAHTFPN-G (cm ⁻¹)		SOCME_TAHOFN-O (cm ⁻¹)		SOCME_TAHTCNB (cm ⁻¹)	
State	$\langle S_0 H_{SO} T_m \rangle^a$	$\langle S_1 H_{SO} T_m \rangle^a$	$\langle S_0 H_{SO} T_m \rangle^a$	$\langle S_1 H_{SO} T_m \rangle^a$	$\langle S_0 H_{SO} T_m \rangle^a$	$\langle S_1 H_{SO} T_m \rangle^a$	$\langle S_0 H_{SO} T_m \rangle^a$	$\langle S_1 H_{SO} T_m \rangle^a$
T1	0.0424	0.036	0.092	0.269	0.045	0.125	0.162	0.01
T2	0.902	0.051	0.06	0.150	0.420	0.021	0.446	0.04
T3	0.189	0.080	0.739	0.276	0.837	0.112	0.014	0.06

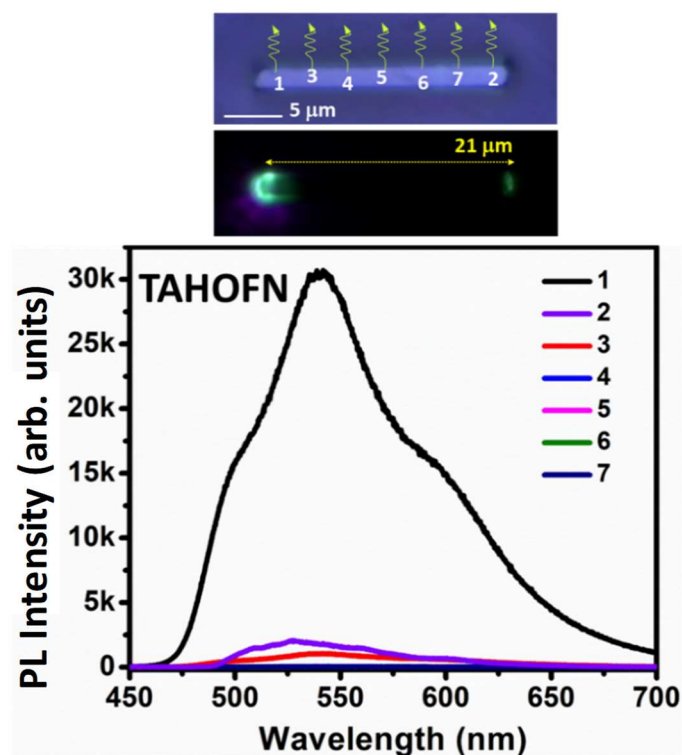
^a $\sqrt{\sum \langle S_n | H_{SO} | T_m \rangle (MS=0,\pm 1)^2}$



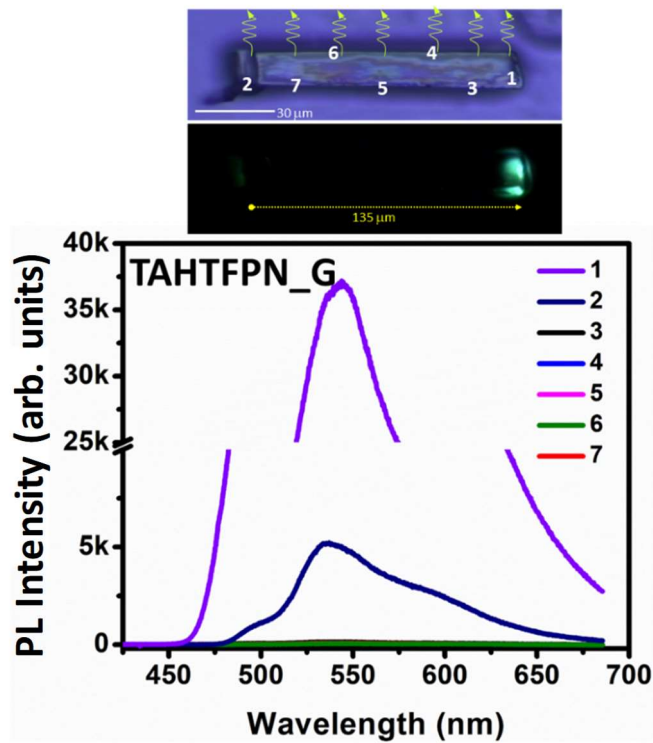
Supplementary Fig. 50: Electron spin resonance (ESR) spectra for TAH (yellow line), TAHOFN (off green line), TAHTFPN_G (green line) and TAHTCNB (red line).



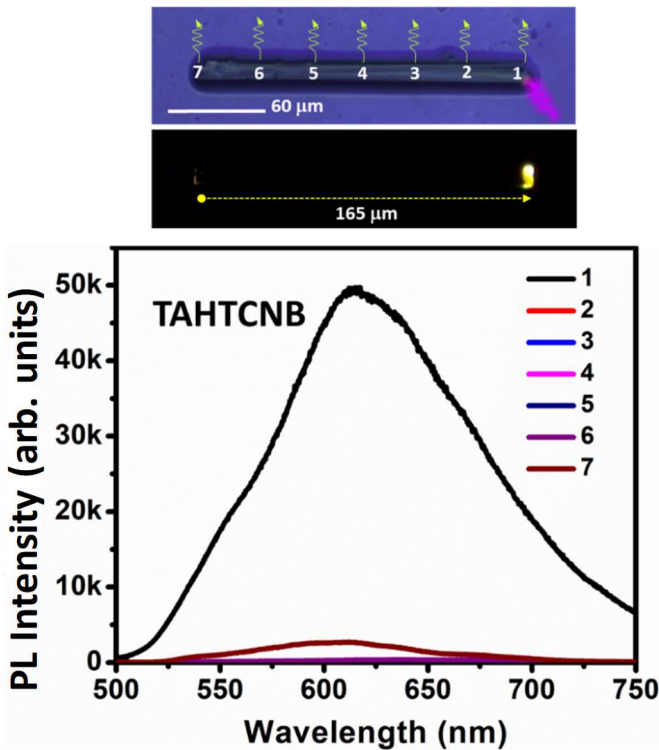
Supplementary Fig. 51: Chemical structures of OFN, TFPN and TCNB molecule, where, x, y, and z are the bond length of carbon-carbon bond at neutral state.



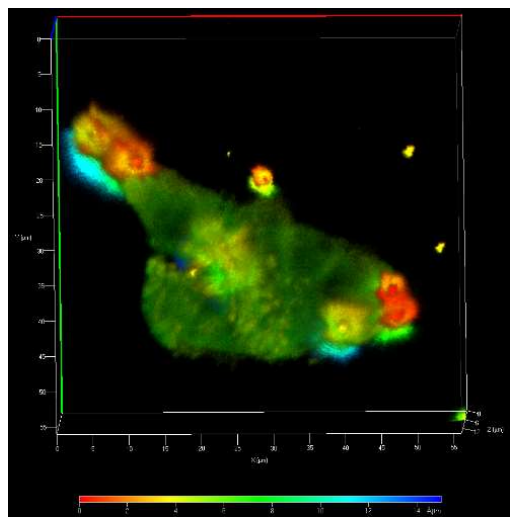
Supplementary Fig. 52: Spatially resolved spectra of TAHOFN crystal: Excitation position was kept constant and PL signals were collected at different positions.



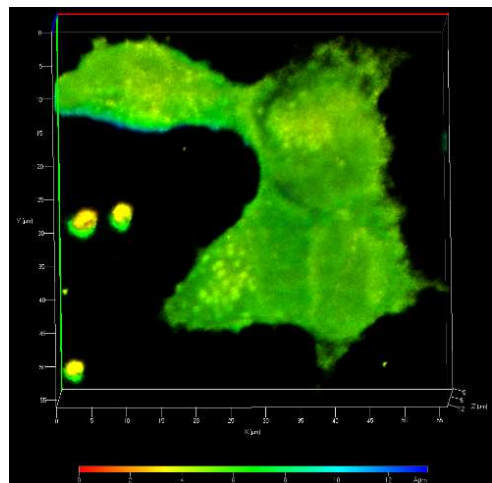
Supplementary Fig. 53: Spatially resolved spectra of TAHTFPN_G crystal: Excitation position was kept constant and PL signals were collected at different positions.



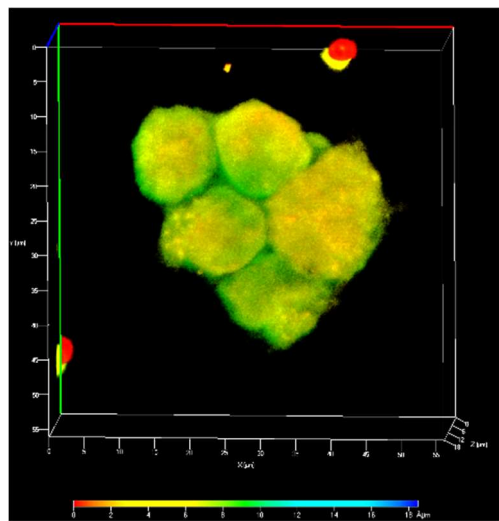
Supplementary Fig. 54: Spatially resolved spectra of TAHTCNB crystal: Excitation position was kept constant and PL signals were collected at different positions.



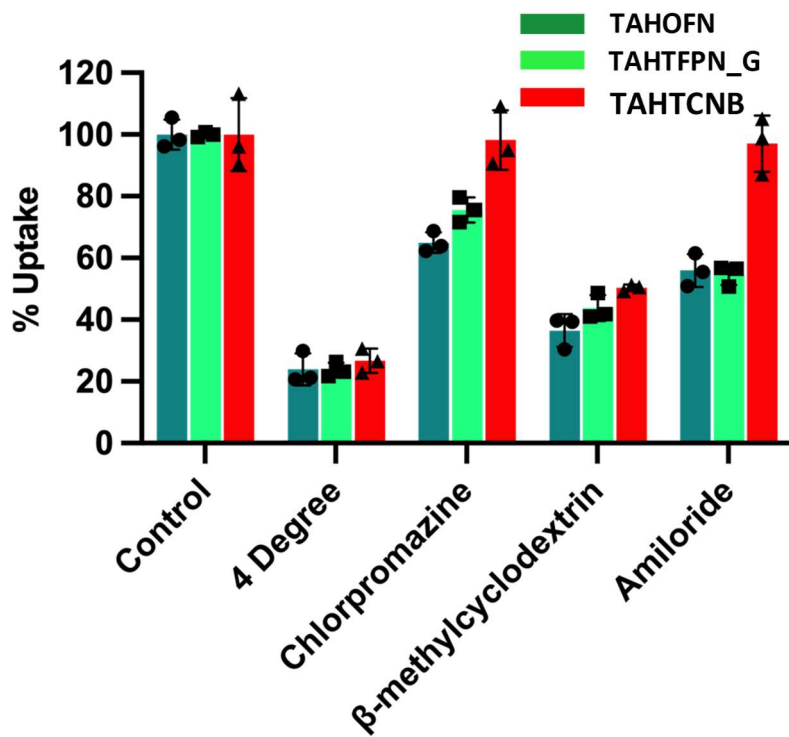
Supplementary Fig. 55: Z-stacking analysis of the MCF-7, confirming the internalization and localization of the TAHOFN in the cytoplasm. (Scale bar: 5 μm).



Supplementary Fig. 56: Z-stacking analysis of the MCF-7, confirming the internalization and localization of the TAHTFPN_G in the cytoplasm. (Scale bar: 5 μm).



Supplementary Fig. 57: Z-stacking analysis of the MCF-7, confirming the internalization and localization of the TAHTCNB in the cytoplasm. (Scale bar: 5 μm).



Supplementary Fig. 58: Cellular internalization mechanism studies using co-crystals. Data are shown as the mean \pm SD ($n=3$). The experimental results shown in this figure was independently replicated three times, demonstrating consistent outcomes.

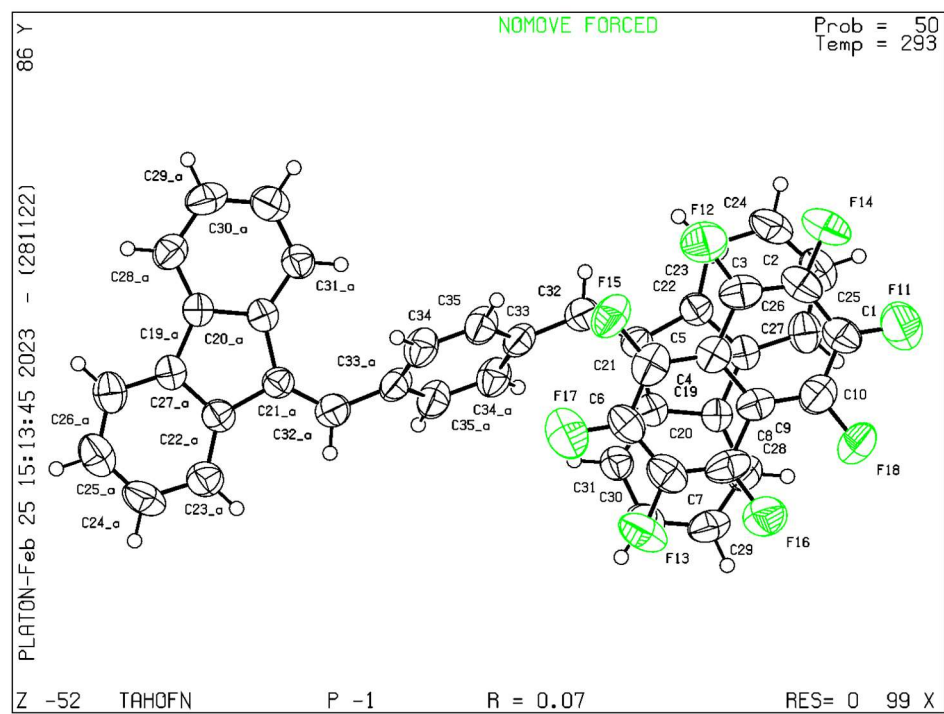
Supplementary Table 24: A brief summary of the previous report on various optically waveguide active molecular crystals.

Name	Emission peak / nm	Fluorescent lifetime / ns	Delayed Fluorescent lifetime / μ s	PLQY	Loss coefficient	Reference
2-acetyl-6dimethylaminonaphthalene (ADN)	450	-	-	-	0.069 dB/ μ m	<i>Angew. Chem., 2013, 125, 8875-8879</i>
2-acetyl-6-methylaminonaphthalene (AMN)	540	-	-	-	0.076 dB/ μ m and 0.457 dB/ μ m along different directions	<i>Angew. Chem., 2013, 125, 8875-8879</i>
2,2'-(5,5'-(3,7-dicyano-2,6-bis(dihexylamino) benzo[1,2 b:4,5-b']difuran 4,8- diyl)bis(thiophe-ne-5,2-diyl)) bis(methanlylidene)dimalononitrile (BDFTM)	676	2.02	-	16%	0.06 dB/ μ m	<i>Adv. Funct. Mater. 2014, 24, 4250-4258</i>
One-dimensional (1D) ribbon-like perylene crystals	580	-	-	5%	0.072 dB/ μ m	<i>J. Mater. Chem. C, 2014, 2, 9695-9700</i>
Two-dimensional (2D) square-like perylene crystals	580	-	-	5%	0.099 and 0.101 dB/ μ m along different directions	<i>J. Mater. Chem. C, 2014, 2, 9695-9700</i>
BDTVA (a 9,10-distyrylanthracene derivative)	509	1.96	-	50%	0.000275 dB/ μ m	<i>ACS Photonics, 2015, 2, 313-318</i>
The cocrystal of trans-1,2-bis(4pyridyl)ethylene and 1,2,4,5tetracyanobenzene	436	6.13	-	19%	0.26 dB/ μ m (isotropic 2D waveguide)	<i>Angew. Chem. Int. Ed., 2015, 54, 6785-6789</i>
The cocrystal of 1,2-di(4pyridyl)ethylene and 1,3,5-trifluoro2,4,6-triiodobenzene	440	1.66	-	26.1%	0.19 dB/ μ m	<i>J. Am. Chem. Soc., 2015, 137, 11038-11046</i>

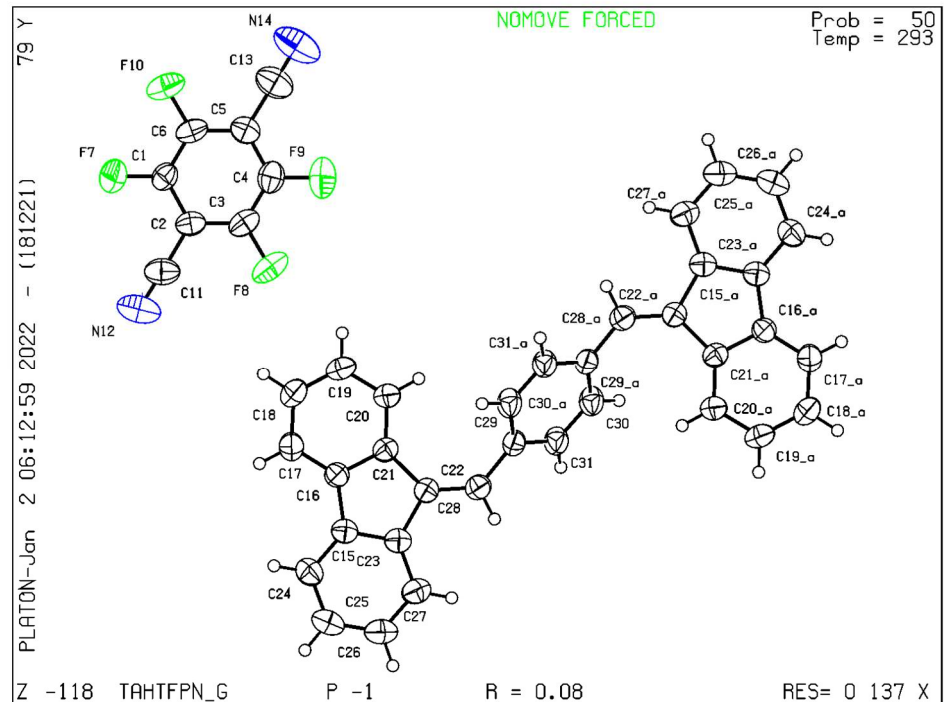
A solvate composed of a carbazole and cyano-substituted tetraphenylethylene derivative cocrystallized with DMF	458	2.45	-	41%	0.00804 dB/ μ m	<i>Small</i> , 2016 , 47, 6554-6561
A solvate composed of a carbazole and cyano-substituted tetraphenylethylene derivative cocrystallized with CHCl ₃	481	1.93	-	65%	0.00708 dB/ μ m	<i>Small</i> , 2016 , 47, 6554-6561
A solvate composed of a carbazole and cyano-substituted tetraphenylethylene derivative cocrystallized with CH ₂ Cl ₂	522	3.01	-	40%	0.00301 dB/ μ m	<i>Small</i> , 2016 , 47, 6554-6561
The cocrystal of 4-(1-naphthylvinyl) pyridine and 1,2,4,5-tetracyanobenzene	about 550	7.5	-	6.8%	0.040-0.11 dB/ μ m	<i>Adv. Mater.</i> , 2016 , 28, 5954-5962
PyB (composed of two chromophores of a pyrene unit and a rhodamine B moiety)	492	6.73	-	3.52%	0.00669 dB/ μ m at 440 nm and 0.00351 dB/ μ m at 497 nm	<i>ACS Appl. Mater. Interfaces</i> , 2017 , 9, 8910-8918
BCZ (a carbazole-containing β diketonate derivative)	567	-	-	37%	0.033 dB/ μ m	<i>Adv. Funct. Mater.</i> , 2017 , 27, 1700332
2,5-dihydro-3,6-bis(octylamino) terephthalate doped with 3,6-bis(octylamino) terephthalate	572	12.7	-	56%	0.000272 dB/ μ m at 576 nm and 0.000196 dB/ μ m at 615 nm	<i>Adv. Mater.</i> , 2018 , 30, 1800814
The cocrystal of 4,4'-(<i>(1E,1'E</i> (2,5dimethoxy-1,4-phenylene)bis(ethene 2,1-diyl))dipyridine and 1,4diiodotetrafluorobenzene	525	-	-	-	0.0145 dB/ μ m at 525 nm for microtubes; 0.0341 dB/ μ m for microrods	<i>J. Mater. Chem. C</i> , 2018 , 6, 9594-9598
7-(diethylamino)coumarin-3-aldehyde	564	8.25	-	7.5%	0.0058 dB/ μ m	<i>Mater. Chem. Front.</i> , 2018 , 2, 910-916
(<i>E</i>)-1-(4-(dimethylamino)phenyl)iminomethyl-2-hydroxyl-naphthalene	615	-	-	43%	0.00027 dB/ μ m for the straight,	<i>Angew. Chem. Int. Ed.</i> , 2018 , 57, 8448 - 8452

					0.000274 dB/ μ m for the bent state	
dimethyl 2,5- bis((2hydroxyethyl)amino)terephthalate	641	6.1	-	8%	0.000351 dB/ μ m for the straight state; 0.000376 dB/ μ m for the bent state	<i>J. Phys. Chem. Lett.</i> , 2019 , 10, 1437- 1442
2,5-dimethoxybenzene- 1,4dicarboaldehyde	499	4.0	-	42%	0.00120 dB/ μ m	<i>ChemPlusChem</i> , 2019 , 84, 247-251
1,4-trimethylsilyl ethynyl anthracene (TMS ANT)	538		-	-	about 0.002 dB/ μ m	<i>Chem. Mater.</i> 2019 , 31, 1775- 1783
1,2,3,4-Tetrafluoro- 5,8bis(trimethylsilyl ethynyl)anthracene (F4 TMS ANT)	559	-	-	-	about 0.0013 dB/ μ m	<i>Chem. Mater.</i> 2019 , 31, 1775- 1783
The 1D cocrystal of fluoranthene and 1,2,4,5-tetracyanobenzene	about 550	80	-	74%	0.0181 dB/ μ m along [100] direction	<i>Nat. Commun.</i> , 2019 , 10, 761
The 2D cocrystal of fluoranthene and 1,2,4,5-tetracyanobenzene	about 550	80	-	74%	0.0084, 0.0139 and 0.0147 dB/ μ m	<i>Nat. Commun.</i> , 2019 , 10, 761
1,4-bis((E)-4- (1,2,2triphenylvinyl)styryl)- 2,5dimethoxybenzene (TPDSB)	526	1.70	-	85.6%	0.012-0.020 dB/ μ m	<i>J. Phys. Chem. Lett.</i> , 2019 , 10, 679-684
Zn-IMDC (IMDC, 4,5- imidazoledicarboxylic acid)	485	-	354.5 ms	2.37%	30-40 dB cm ⁻¹	<i>Sci. Bull.</i> 2022 , 67, 2076- 2084
(4,4'-bis(2,5-dimethylstyryl)biphenyl, Bdb)	460	1.56	-	82.49%	-	<i>Sci China Chem</i> , 2022 , 65, 408-417.
The 1D cocrystal of 9-anthracene carboxylic acid and 1,2,4,5tetracyanobenzene (9AC-TCNB)	583 and 652	$\tau_1 = 2.38$ ns (40.63%) and $\tau_2 = 6.71$ ns (59.31%)	-	-	0.006706 dB/ μ m at 583 nm; 0.006602	<i>Adv. Opt. Mater.</i> , 2020 , 8, 1901280

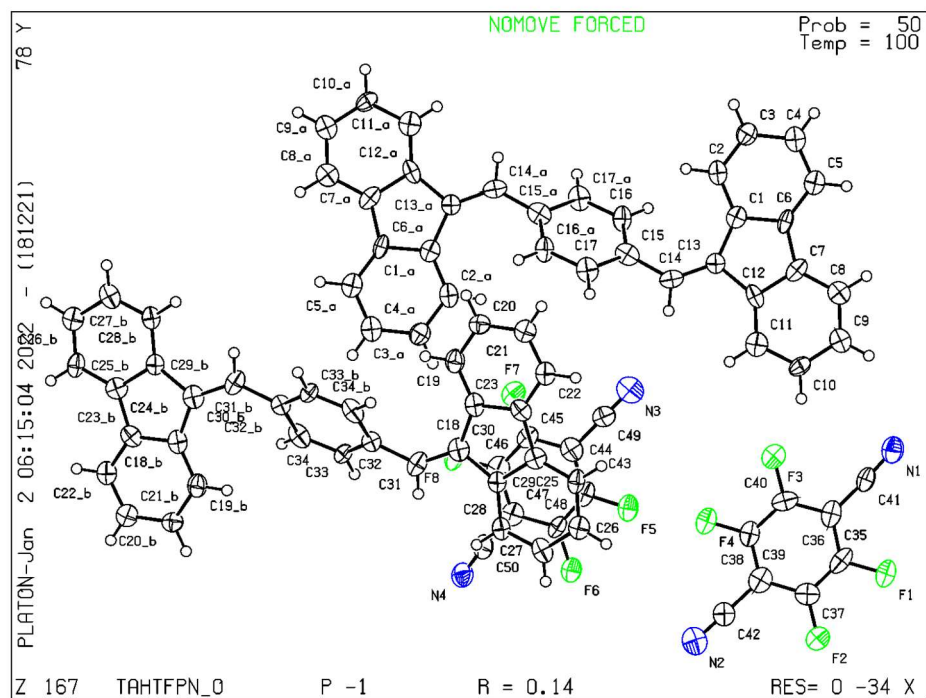
		at 583 nm; τ = 5.87 ns (96.69%) at 652 nm			dB/ μm at 652 nm	
The 2D cocrystal of 9-anthracene carboxylic acid and 1,2,4,5-tetracyanobenzene (9AC-TCNB)	650	-	-	-	0.0068306 dB/ μm at 650 nm	<i>Adv. Opt. Mater.</i> , 2020 , 8, 1901280
One of polymorphic 2D cocrystals composed of 4-(4-dimethylaminostyryl)quinolone and 1,4-diiodotetrafluorobenzene (MDFCs)	515	0.24	-	12%	0.0140 dB/ μm , 0.0520 dB/ μm and 0.0540 dB/ μm along different directions	<i>Angew. Chem. Int. Ed.</i> , 2020 , 59, 44564463.
One of polymorphic 2D cocrystals composed of 4-(4-dimethylaminostyryl)quinolone and 1,4-diiodotetrafluorobenzene (TDFCs)	565	1.91	-	11%	0.104 dB/ μm , 0.115 dB/ μm and 0.108 dB/ μm	<i>Angew. Chem. Int. Ed.</i> , 2020 , 59, 44564463.
Tri-phenylene (TP)-2,3,5,6-tetrafluoro-7,7,8,8-tetracyanoquinodimethane (F4TCNQ) CT organic complex	770	11.3 ns	-	5.4%	0.060 dB μm^{-1}	<i>Adv. Mater.</i> 2022 , 34, 2107169.
Trans-1,2-Diphenylethylene and 1,2,4,5-tetracyanobenzene	580	31.5 ns	$\tau_1 = 0.69 \text{ ms}$ and $\tau_2 = 2.94 \text{ ms}$	13.77%	-	<i>Angew. Chem. Int. Ed.</i> , 2019 , 58, 11311 – 11316.
Calix[3]acridan (C[3]A) and 1,2-dicyanobenzene (DCB)	500	152 ns	5.2 μs	70%	-	<i>Angew. Chem. Int. Ed.</i> , 2022 , 61, e202117872.
Through-space cocrystals of twisted aromatic hydrocarbon (TAH) donor and octafluoronaphthalene (OFN), tetrafluoropterophenonitrile (TFPN) and 1,2,4,5-tetracyanobenzene (TCNB) denoted as TAHOFN, TAHTFPN_G, TAHTFPN_O and TAHTCNB	540 545 560 590	0.50 ns 0.87 ns 1.06 ns 38.81 ns	5.38 μs 74.4% 77.5% 64.4%	31.6% 0.44 dB/ μm , 0.0742 dB/ μm 0.0837 dB/ μm	OWG loss coefficient:	Present work



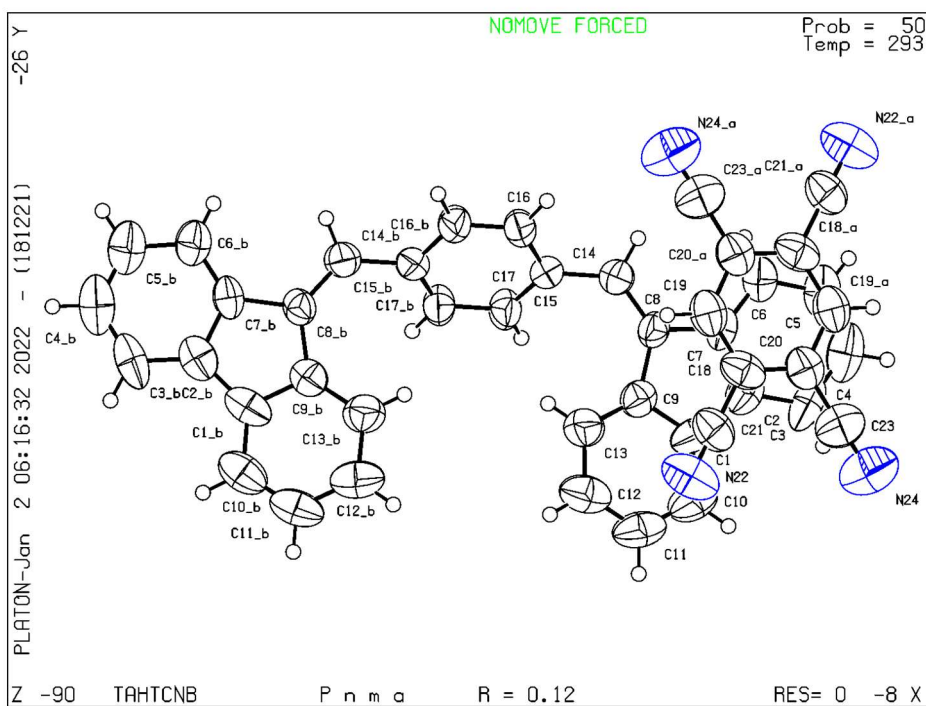
Supplementary Fig. 59: An ellipsoid figure of TAHOFN single crystal structure.



Supplementary Fig. 60: An ellipsoid figure of TAHTFPN_G single crystal structure.



Supplementary Fig. 61: An ellipsoid figure of TAHTFPN_O single crystal structure.



Supplementary Fig. 62: An ellipsoid figure of TAHTCNB single crystal structure.

Supplementary Table S25. Cartesian coordinates of TAHOFN used for the TD-DFT calculation at B3LYP/6-31G (d,p) level.

F	1.20431400	-0.97743800	-2.11241400
F	3.17325900	-2.59372200	-1.84605200
F	5.78097100	-2.96327900	-1.35622500
F	4.48512800	3.23772600	-1.08012000
F	1.88924100	3.62637900	-1.54609700
F	6.43361500	1.63635100	-0.71945600
F	0.27026300	1.53800200	-2.02086400
F	7.37254500	-0.88129700	-0.79234400
C	3.38144400	-0.19845600	-1.58978300
C	4.28018400	0.85274300	-1.30548200
C	1.53600900	1.31496100	-1.80169800
C	3.96029000	-1.53478200	-1.60066900
C	5.25771000	-1.72345500	-1.34427000
C	6.11256700	-0.65615300	-1.06160500
C	2.05610600	0.04086000	-1.84881400
C	2.40432900	2.36254800	-1.54657900
C	5.60412100	0.61150900	-1.03561400
C	3.69183600	2.18319200	-1.31080400
C	1.90426300	0.74738500	1.72997200
C	3.27785000	0.83658900	2.02533100
C	3.85482700	-0.50649300	1.99803100
C	1.57732900	-0.68081600	1.47135700
C	2.84147500	-1.40859700	1.65406300
C	1.15606700	1.90702300	1.63700800
H	0.25140300	1.86347100	1.42573000
C	0.42259700	-1.24641900	1.07892900
H	0.48866800	-2.14514400	0.84812300
C	-0.91838100	-0.67964100	0.95746400
C	-2.95772600	-0.42329100	-0.30447200
H	-3.43619800	-0.57974400	-1.08714700
C	5.14746100	-0.95876700	2.23196600

H	5.82219200	-0.35805200	2.45579500
C	-1.67619800	-0.91200300	-0.18901400
H	-1.31045400	-1.40623000	-0.88694500
C	1.75915300	3.13124700	1.85977800
H	1.25450800	3.91065200	1.80201200
C	3.12990400	-2.76521000	1.56252800
H	2.45986300	-3.37545700	1.34898300
C	3.87186000	2.06300800	2.24844900
H	4.77739700	2.11479000	2.45189300
C	3.11252800	3.21314500	2.16800500
H	3.50502800	4.04102000	2.32127500
C	4.42461400	-3.19858200	1.79337900
H	4.62612400	-4.10432600	1.72271300
C	5.42260700	-2.29793300	2.13030400
H	6.28601700	-2.60394400	2.28845200
C	-6.37498500	-1.12899900	-0.04914000
C	-7.74857100	-1.21820200	-0.34449800
C	-8.32554900	0.12488000	-0.31719800
C	-6.04805200	0.29920300	0.20947600
C	-7.31219800	1.02698400	0.02676900
C	-5.62679000	-2.28863600	0.04382400
H	-4.72212500	-2.24508400	0.25510300
C	-4.89332000	0.86480600	0.60190300
H	-4.95939000	1.76353100	0.83270900
C	-3.55234100	0.29802700	0.72336800
C	-1.51299700	0.04167700	1.98530500
H	-1.03452500	0.19813100	2.76798000
C	-9.61818400	0.57715300	-0.55113400
H	-10.29291400	-0.02356200	-0.77496200
C	-2.79452400	0.53039000	1.86984600
H	-3.16026900	1.02461600	2.56777800
C	-6.22987500	-3.51286000	-0.17894500
H	-5.72523100	-4.29226400	-0.12117900
C	-7.60062600	2.38359600	0.11830500

H	-6.93058500	2.99384400	0.33184900
C	-8.34258300	-2.44462100	-0.56761700
H	-9.24811900	-2.49640400	-0.77106100
C	-7.58324900	-3.59475800	-0.48717300
H	-7.97575000	-4.42263400	-0.64044200
C	-8.89533500	2.81696900	-0.11254600
H	-9.09684600	3.72271300	-0.04188100
C	-9.89332800	1.91631900	-0.44947200
H	-10.75673900	2.22233000	-0.60762000

Supplementary Table S26. Cartesian coordinates of TAHTFPN_G used for the TD-DFT calculation at B3LYP/6-31G (d,p) level.

C	-1.33669100	-0.59839500	0.19057000
H	-0.96262300	-1.41801500	-0.03945300
C	3.31147400	0.28780200	1.50708800
C	1.55918900	3.23059900	0.04910000
H	0.66665200	3.07125100	-0.15859500
C	4.33144200	1.28847600	1.41853600
C	4.92157000	-1.21922800	2.37414700
H	5.14898500	-2.06525900	2.68591200
C	-0.51360800	0.40473200	0.75170000
C	5.61499500	1.00592800	1.81215100
H	6.28183200	1.64912300	1.74198400
C	-2.67780300	-0.38547900	-0.02278100
H	-3.19352300	-1.05715300	-0.40587200
C	3.69963200	2.49527600	0.87864300
C	3.62821900	-0.97952100	1.99126700
H	2.97987900	-1.64470700	2.05340500
C	5.89788900	-0.24343400	2.31100500
H	6.75762200	-0.43582700	2.61036200
C	2.32390400	2.23396300	0.63190900
C	0.90727000	0.09091200	1.02418400
H	1.05623200	-0.80353000	1.23014100

C	2.05380600	0.85317900	1.03522200
C	4.25775500	3.73486100	0.59938100
H	5.15429100	3.89654000	0.78111300
C	2.12239200	4.46848500	-0.22634600
H	1.60116500	5.14135000	-0.59934600
C	3.48113200	4.71210000	0.05671000
H	3.84840800	5.54620100	-0.12864700
C	-2.46173600	1.84533800	0.89220300
H	-2.83580500	2.66495800	1.12222600
C	-7.10990100	0.95914100	-0.42431400
C	-5.35761700	-1.98365600	1.03367400
H	-4.46508000	-1.82430800	1.24136900
C	-8.12987000	-0.04153300	-0.33576200
C	-8.71999700	2.46617100	-1.29137300
H	-8.94741300	3.31220200	-1.60313800
C	-3.28482000	0.84221100	0.33107400
C	-9.41342200	0.24101500	-0.72937700
H	-10.08026000	-0.40218000	-0.65921100
C	-1.12062500	1.63242200	1.10555500
H	-0.60490500	2.30409600	1.48864500
C	-7.49806000	-1.24833300	0.20413100
C	-7.42664700	2.22646400	-0.90849300
H	-6.77830600	2.89165000	-0.97063100
C	-9.69631600	1.49037700	-1.22823100
H	-10.55605000	1.68277000	-1.52758900
C	-6.12233200	-0.98702000	0.45086400
C	-4.70569800	1.15603200	0.05859000
H	-4.85466000	2.05047300	-0.14736800
C	-5.85223400	0.39376400	0.04755200
C	-8.05618300	-2.48791800	0.48339300
H	-8.95271800	-2.64959700	0.30166100
C	-5.92082000	-3.22154200	1.30911900
H	-5.39959300	-3.89440700	1.68212000
C	-7.27955900	-3.46515700	1.02606400

H	-7.64683600	-4.29925800	1.21142000
F	5.59008400	-3.61330100	-0.21460900
F	6.98431200	-1.35209600	-0.57411100
F	1.70121000	-1.49673700	-1.84616200
F	3.14664300	0.76780700	-2.24909500
N	2.41624700	-4.85772200	-0.78239300
N	6.52429900	1.86404500	-1.88372800
C	2.91639300	-3.82657900	-0.90088400
C	3.02399400	-1.47020400	-1.54644500
C	3.63633300	-2.60039600	-1.04201500
C	5.88283500	0.93099000	-1.66341500
C	4.99513000	-2.54639800	-0.71464200
C	5.08548500	-0.25513300	-1.43069300
C	3.74391800	-0.31907600	-1.74878800
C	5.68896000	-1.36318400	-0.90891000

Supplementary Table S27. Cartesian coordinates of TAHTFPN_O used for the TD-DFT calculation at B3LYP/6-31G (d,p) level.

F	9.33991505	-2.17941218	-0.01933637
F	8.49587813	-4.71810680	0.13040608
F	4.89415717	-0.72459117	-0.39469103
F	4.05254108	-3.26459618	-0.28671592
C	7.13181471	-1.39957737	-0.19126929
C	8.03328673	-2.44104707	-0.05364994
C	7.59863784	-3.73678116	0.00823376
C	5.78828802	-1.70376792	-0.25854922
C	6.25385494	-4.04447945	-0.05510540
N	7.97728734	1.02946227	-0.34273084
C	7.59012189	-0.04052310	-0.27462742
C	5.35139584	-3.00067634	-0.20227769
C	5.77742740	-5.39697473	0.01990378
N	5.40954295	-6.46405451	0.10723481
C	0.19510833	5.48696190	0.02212601

C	-0.25386017	4.07098387	0.06025007
C	1.58838067	5.53739106	0.13987120
C	0.99605072	3.27179863	0.20017973
C	2.08680070	4.16440908	0.25053731
C	-1.54088615	3.71044816	-0.07896366
H	-2.11716597	4.42027408	-0.25153237
C	-2.20660998	2.40592888	-0.00867103
C	1.24432686	1.90375125	0.19347758
H	0.54211432	1.29845713	0.11894741
C	-3.25105781	2.11781889	-0.88349820
H	-3.49889675	2.74975253	-1.51878047
C	-0.53759245	6.65999355	-0.11293926
H	-1.46392939	6.63307367	-0.18559525
C	2.25654661	6.75456372	0.12342767
H	3.18218938	6.78779928	0.20780573
C	0.13502767	7.86738267	-0.13888995
H	-0.34576414	8.65728127	-0.23685487
C	-3.92250976	0.92459123	-0.82995729
H	-4.60559023	0.75810737	-1.43770527
C	3.38381273	3.69805290	0.35151125
H	4.09574362	4.29480974	0.39661010
C	3.61087211	2.33804497	0.38438451
H	4.47882911	2.01481062	0.46493660
C	1.51634481	7.91997734	-0.02035519
H	1.95054552	8.74224570	-0.03812612
C	2.55202927	1.45347821	0.29916364
H	2.71956709	0.53901454	0.31329860
C	-5.99952595	-3.12762111	0.09137480
C	-5.55055757	-1.71164404	0.05325061
C	-7.39279837	-3.17805010	-0.02637138
C	-6.80046847	-0.91245881	-0.08667905
C	-7.89121856	-1.80506912	-0.13703761
C	-4.26353156	-1.35110722	0.19246349
H	-3.68725188	-2.06093412	0.36503208

C	-3.59780775	-0.04658906	0.12217172
C	-7.04874446	0.45558956	-0.07997677
H	-6.34653192	1.06088368	-0.00544660
C	-2.55335992	0.24152094	0.99699889
H	-2.30552098	-0.39041271	1.63228116
C	-5.26682515	-4.30065276	0.22644007
H	-4.34048821	-4.27373284	0.29909606
C	-8.06096423	-4.39522293	-0.00992686
H	-8.98660711	-4.42845834	-0.09430591
C	-5.93944528	-5.50804189	0.25239076
H	-5.45865356	-6.29794032	0.35035470
C	-1.88190784	1.43474958	0.94345810
H	-1.19882749	1.60123359	1.55120509
C	-9.18823047	-1.33871308	-0.23801057
H	-9.90016135	-1.93546879	-0.28311028
C	-9.41528984	0.02129485	-0.27088382
H	-10.28324684	0.34452920	-0.35143591
C	-7.32076253	-5.56063750	0.13385588
H	-7.75496325	-6.38290476	0.15162595
C	-8.35644696	0.90586274	-0.18566381
H	-8.52398469	1.82032626	-0.19979779

Supplementary Table S28. Cartesian coordinates of TAHTCNB used for the TD-DFT calculation at B3LYP/6-31G (d,p) level.

C	1.63148405	1.21532597	0.85740622
C	1.95876617	-0.21160838	1.20535204
C	3.36749467	-0.18823736	1.70545831
C	3.82059749	1.15423151	1.70411015
C	-0.25017040	-1.44115189	0.89192368
C	1.19878805	-1.31775405	1.13176087
C	-1.15276279	-0.65435814	1.56306004
C	0.50575998	1.78261518	0.25299394
C	2.75880993	1.99678519	1.15424080

C	4.15822365	-1.20230540	2.17310712
C	-0.76886772	-2.40566972	0.03041494
C	5.10704425	1.42298850	2.18774410
C	5.43895383	-0.90060013	2.62961701
C	0.52274503	3.15627162	-0.01220688
C	1.62849410	3.92454302	0.34505578
C	2.73325092	3.37223235	0.91263167
C	5.90059711	0.36812841	2.62681298
H	3.46281197	3.90344160	1.13724159
H	1.61032072	4.84149229	0.19085411
H	-0.20598305	3.55743980	-0.42803910
H	-0.23297258	1.26201708	0.03354117
H	3.84575774	-2.07813545	2.18591544
H	5.98572204	-1.58504027	2.94184252
H	6.76493527	0.54002340	2.92387090
H	5.42691647	2.29582678	2.21505136
H	1.65260855	-2.12098250	1.24910901
H	-0.84166536	-0.03151078	2.17965088
H	-0.18812000	-2.98618756	-0.40620096
C	-5.20909998	0.65499827	-0.24284264
C	-5.39773505	-0.81419603	0.02212236
C	-6.87707582	-1.02739328	0.05770764
C	-7.51415660	0.22577619	-0.11898714
C	-3.03547231	-1.66930226	0.44393193
C	-4.48729177	-1.78351370	0.21720404
C	-2.52374686	-0.76665855	1.34254910
C	-4.05612192	1.40894112	-0.48074536
C	-6.48174464	1.23987048	-0.33202258
C	-7.60270779	-2.16566987	0.28146289
C	-2.12809183	-2.51700684	-0.18820451
C	-8.91273216	0.27459693	-0.06721584
C	-8.99270492	-2.08272992	0.30840936
C	-4.20735460	2.76881846	-0.77300255
C	-5.47651700	3.34255550	-0.79772389

C	-6.60075158	2.60766311	-0.58866201
C	-9.62563430	-0.90366029	0.12955277
H	-7.43852775	3.01048823	-0.61614474
H	-5.55693062	4.25440653	-0.96193637
H	-3.45871371	3.29100128	-0.95121273
H	-3.21304319	1.01791276	-0.44577744
H	-7.17499435	-2.98087016	0.41332266
H	-9.49364861	-2.85299050	0.45211946
H	-10.55524543	-0.87871174	0.13806944
H	-9.35940719	1.08464560	-0.16320108
H	-4.82159586	-2.65129921	0.20778915
H	-3.10611972	-0.21699735	1.81543296
H	-2.44406978	-3.17097750	-0.76905100
C	5.17760568	0.52991943	-1.33330488
C	3.90737749	0.53616979	-1.89971368
N	2.80989919	2.71575885	-2.70620973
C	3.29591895	1.75404110	-2.34564912
C	3.20805823	-0.66848800	-2.08640062
C	5.89494443	1.74801136	-1.12814402
N	6.48103300	2.70149154	-0.96080579
H	2.35998440	-0.65495722	-2.46779975
C	3.77262430	-1.87863384	-1.70625835
C	5.04285250	-1.88488420	-1.13984955
N	6.14033080	-4.06447326	-0.33335350
C	5.65431103	-3.10275551	-0.69391411
C	5.74217176	-0.68022641	-0.95316261
C	3.05528553	-3.09672577	-1.91141920
N	2.46919697	-4.05020595	-2.07875744
H	6.59024561	-0.69375719	-0.57176348

Supplementary References

- (1) Material Studio 8.0, Accelrys Inc., San Diego, 2014.
- (2) Spackman, M. A. & Jayatilaka, D. Hirshfeld surface analysis *CrystEngCom.*, **11**, 19–32 (2009).
- (3) Spackman, M. A.; McKinnon, J. J.; Jayatilaka, D. *CrystEngComm.* **10**, 377–388 (2008).
- (4) Frisch, M. J. et al. Gaussian, Inc., Wallingford CT, 2016.
- (5) Salla, C. A. M. et al. *Angew. Chem., Int. Ed.*, **58**, 6982– 6986, (2019).